Rapid Electronic Diagnostics of Ebola Virus with Synthetic Nanobody-Conjugated Gold Nanoparticles

Xiahui Chen[1,2,3], Shoukai Kang[4,5], Ashif Ikbal[1,2,3], Zhi Zhao[1,2,6], Jiawei Zuo[1,3], Yu Yao[1,3], Liangcai Gu[4,5], Chao Wang[1,2,3*]*

[1]School of Electrical, Computer and Energy Engineering, Arizona State University, Tempe, AZ 85287, USA

[2]Center for Molecular Design and Biomimetics at the Biodesign Institute, Arizona State University, Tempe, AZ 85287, USA

[3]Centre for Photonic Innovation, Arizona State University, Tempe, AZ 85287, USA

[4]Department of Biochemistry, University of Washington, Seattle, WA 98195, USA

[5]Institute for Protein Design, University of Washington, Seattle, WA 98195, USA

[6]Current Address: College of Materials Science and Engineering, Key Laboratory of Advanced Functional Materials, Education Ministry of China, Beijing University of Technology, Beijing 100124, China

KEYWORDS: Ebola virus glycoproteins, metal nanoparticles, colorimetric sensing, point-of-care test

ABSTRACT:

The success of controlling emerging infectious diseases relies on the fast development of robust, quantitative assays for point-of-care testing. Here a generalizable strategy is demonstrated for developing inexpensive, simple-to-use, and rapid diagnostics within a few weeks upon the identification of a new viral antigen. Using Ebola virus secreted glycoprotein (sGP) as a target, we design a new assay featuring nanobody-conjugated nanoparticles for rapid, electronic detection (Nano2RED). Nanobodies with the high affinity and specificity were generated by phage display screening of a high-quality combinatorial library (> 10^9) and site-specifically conjugated to gold nanoparticles (AuNPs) for in-solution colorimetric detection. Our assay can robustly detect the sGP protein from 10 pM to 100 nM in diluted serum and distinguish it from a membrane-anchored isoform, GP1,2, allowing the diagnosis of the viral infection stage. Additionally, a rapid assay protocol was established to decrease the assay time to a few minutes without compromising the accuracy. Lastly, this assay has been integrated with a portable semiconductor device with a digital readout and minimal training requirement for end users. Our method can be widely applied to the point-of-care testing of other infectious diseases.

In the recent past, we have witnessed the emergence of many infectious viral diseases, from highly fatal Ebola virus disease (EVD, fatality rate from 45% to 90%) [1, 2] to most recently highly contagious coronavirus disease 2019 (COVID-19), which has recorded over 120 million infections and 2.7 million deaths reported globally[3]. Future emergence of Disease X, *e.g.* something as contagious as COVID-19 and as lethal as EVD, could pose even greater threat to humanity but remains extremely difficult to prevent or predict. Upon the disease emergence, early pathogen identification and infection isolation are viewed crucially important in containing the disease transmission[4]. Therefore, it is necessary to accelerate the diagnostic system design, development, and validation process and make them broadly accessible within weeks from the first outbreak for effective mitigation[4]. Current diagnostic methods rely on the detection of the genetic (or molecular), antigenic, or serological (antibody) markers [5]. Genetic diagnostics use sequencing, polymerase amplification assays, and most recently CRISPR technologies [6, 7]. For example, real-time reverse transcription polymerase chain reaction (RT-PCR) tests are viewed the gold standard in diagnostics for their high sensitivity; however, they are also comparatively more costly, time-consuming and instrument-demanding, due to inherent sample extraction and nucleic acid amplification processes. Genetic tests may also suffer from false negatives due to sample handling and virus mutations and often display a long tail of false positives by picking up genetic fragments from inactive viruses [8]. In comparison, antigen and antibody detections are complementary as they allow more rapid and point-of-care (POC) detection without complex sample preparation or amplification, thus suitable for surveillance and timely isolation of highly infectious individuals, particularly outside clinical settings [8]. While antibody (*e.g.* IgM) detections can be potentially feasible for disease diagnostics [9], they are less predictive and most suitable for immune response studies. In comparison, viral protein antigen tests provide a reliable field-test solution in

diagnosing symptomatic patients[9-11] , and may serve to screen asymptomatic contacts that may become symptomatic [12]. In addition, being rapid, easy-to-operate and low-cost, antigen tests can be deployed at high frequencies and large volumes for in-time surveillance [8], which is important to disrupting virus transmission chain.

Current antigen diagnostics typically employ enzyme-linked immunosorbent assays (ELISA) and lateral flow immunoassays (LFIs). ELISA is the workhorse immunochemical test to analyze antigens and antibodies, but requires a multistep workflow and a series of washing steps, hours of incubation prior to readout, and readout system dependent on conversion of a chemical substrate and limited by a narrow linear range (~2 logs) for the optical density. Deployment of ELISAs in high-throughput mass screenings requires automated liquid handling systems to coordinate the complex workflow, thus non-ideal for portable and POC uses. LFIs are potentially much easier to use in a POC setting but usually have much lower sensitivity and thus poorer accuracy compared to ELISA [12]. Here we report a standardized strategy that can quickly establish a rapid, POC antigen diagnostic tool within weeks from the pathogen identification, *i.e.* nanobody-conjugated nanoparticles for rapid, electronic detection (Nano2RED), which has a sensitivity and dynamic range better than ELISA and a portable electronic readout. Here, single-domain antibodies or nanobodies are selected against target antigens using an ultra-fast, animal immunization-independent phage selection method and to preserve the protein quality, site-specifically biotinylated and immobilized onto gold nanoparticles (AuNPs). The nanobody-conjugated AuNPs are ready for a colorimetric assay ideally suited for rapid detection of antigens. Using HEK293 cell expressed secreted Ebola virus glycoprotein (sGP) as the target antigen, we selected high-affinity nanobodies (equilibrium dissociation constant, K_D = 4.63 nM), and demonstrated to detect sGP in diluted serum at a concentration as low as 4.6 ng/ml (~42 pM), well

below at the clinical relevant μg/ml level in patient's blood [13-17]. The sensitivity of our Nano2RED assay was shown to be ~19 fold higher than ELISA using the same antigen and nanobody proteins (0.8 nM), and is expected ~40 folds higher than lateral flow assays (hundreds of ng/ml [18, 19]). Unlike other tests that require amplification (*e.g.* genetic tests) or give only qualitative readouts (*e.g.* LSIs), our assay is quantitative with the dynamic range of > 5 logs and thus suitable for evaluation of patients' viral load, which is crucial to treatment management as it can serve to understand disease severity and predict clinical outcome. The portability, low cost, and simplicity in use features of our assay make it suitable for frequent testing and POC use, which is important to identification of infectious patients and interruption of the transmission chains. Lastly, the electronic readout capability of our assay can be extended to automate data collection, storage, and analysis, further reducing health care workers' workload and speeding up diagnostic and surveillance response.

Nanobody selection

To demonstrate ultrafast, animal immunization-independent generation of high-quality affinity reagents with a significantly lower protein production cost than traditional antibodies, we chose to use nanobodies, ~12-15 kDa functional antibody fragments from camelid comprising a universal scaffold and three variable complementarity-determining regions (CDRs), which are ideally suited for phage display selection and low-cost bacterial production [20]. To avoid relatively lengthy and costly procedures and animal protection issues associated with traditional antibody screening, we obtained nanobodies by screening a vastly diverse synthetic combinatorial library (>10^9) constructed with an optimized thermostable scaffold in our previous report[21]. The target protein

sGP is a 110 kDa homodimeric isoform of the glycoproteins encoded by a GP gene of all five species of Ebolavirus with multiple post-translational modificiations[14]. sGP is believe to act as decoys to disrupt the host immune system by absorbing anti-GP antibodies [14, 22]. Given its abundance in blood stream upon infection and its quantitative correlation with disease progression and humoral response, sGP is widely used as a circulating biomarker in EBOV diagnostics [22, 23]. To obtain high-affinity anti-sGP nanobody, three rounds of biopanning were performed using our combinatorial nanobody library and the HEK293 cell-expressed and secreted recombinant sGP bearing an AviTag for enzymatic biotinylation and bead immobilization (Figure 1a, Figure S1a). After round three, 10 candidates out of 96 randomly picked clones (Figure S1b) were bacterially expressed as a C-terminal His-tag and Avi-tag fusion for subsequent purification and biotinylation. Among them, sGP49 showed the highest binding affinity (K_D = 4.63 nM by bio-layer interferometry; Figure S1c) and the highest production yield (> 5 mg per liter of culture). Of note, the whole selection and protein production process took less than three weeks and the timeline should be applicable to generating nanobody binders against other antigens.

Nanobody-conjugated nanoparticles for rapid, electronic detection (Nano2RED)

Plasmonic metal nanoparticle (MNP) based assays have been applied to detecting multiple species of analytes from smallest molecules to large cells through a variety of signal transduction mechanisms, *e.g.*, surface plasmon resonance, surface enhance Raman spectra, AuNP enhanced fluorescent, colorimetry, scanning electron microscope (SEM) and so on[24-28]. Here in our Nano2RED assay design, AuNPs are conjugated with synthesized nanobodies to form multivalent sensors that aggregate at the presence of specific antigen and subsequently precipitate, thus producing antigen-concentration-dependent signals that can be generated within minutes and

readily quantified by optical and electronic readout. In particular, the AuNP sensors were surface-coated with streptavidin by first self-assembly thiolated carboxyl poly(ethylene glycol) linker via thiol-sulfide reaction and then functionalization of streptavidin via amine-carboxyl coupling. Then biotinylated nanobodies (sGP49) were mixed with AuNPs, followed by filtration to remove excessive nanobodies, to form the antibody-rendered AuNPs for detection (Figure 1a and 1b). Taking ~80 nm AuNP as an example, there are estimated up to ~460 bound sGP49 nanobodies on the AuNP surface, rendering a strong multivalent binding capability that is highly favorable in AuNP aggregation even at low antigen concentration.

In our proposed sensing mechanism (Figure 1b), all the AuNP monomers are initially uniformly dispersed in colloid, presenting a reddish color from characteristic localized surface plasma resonance (LSPR) extinction[29]. Upon mixing with sGP antigen, multiple AuNP monomers bridge through the sGP-sGP49 binding, and gradually form large aggregates. Compared to AuNP monomers, the formation of AuNP aggregates gradually shifts LSPR extinction to higher wavelength attributed to a more collective plasma resonance, leading to achromatic color presentation[30]. Meanwhile the extinction cross section for aggregates with increased size drops assuming constant gold mass density, according to our finite difference time domain (FDTD) simulations (Figure S2). Both factors lead to the colloid to become more transparent. These large AuNP aggregates quickly precipitate at the bottom of the assay container as the gravity force overwhelms the fluidic drag force (Figure 1c-d). As a result, decreased concentration of AuNP monomers in the upper supernatant of centrifuge tube leads to significant color intensity change, corresponding to different sGP concentrations (Figure 1d). Such a color change in the supernatant can be directly visualized by bare eyes, or more quantitatively in a well plate through spectrometric readout or alternatively using electronic readout that analyzes the AuNP absorption.

Impact of nanoparticle size on sGP sensing in phosphate buffered saline (PBS) buffer

The size and shape of AuNPs not only determine the optical extinction and therefore the suspension color, but also directly affect the sensitivity and assay time. Here, the AuNP size effect was studied with NP diameters of 40, 60, 80 and 100 nm in sensing of Ebola sGP proteins from 1 pM to 1 μM in 1× PBS buffer (Figure 2). To standardize the measurement, the sGP signals were collected using a UV-visible spectrometer coupled to an upright microscope (Figure S3a). We custom-designed a polydimethylsiloxane (PDMS) well plate, consisting of 2 mm diameter and 3 mm thick punched holes, that is bonded to a 1 mm thick glass slide as the sample cuvette (Figure S3b). Supernatant sGP samples (5 μL) from an Eppendorf tube were loaded into the PDMS wells and sealed with a 100 μm thick cover glass to avoid buffer evaporation. Additionally, the AuNP concentrations were adjusted to have roughly identical optical density level at their peak plasmonic resonance wavelength (533, 544, 559 and 578 nm for 40, 60, 80 and 100 nm diameter), at an AuNP concentration $[NP]$ of 0.275, 0.086, 0.036 and 0.019 nM, respectively. The extinction coefficient of NPs is theoretically proportional to their total mass (or volume) as $\sigma_{ext} \propto [NP]d^3$ [31], therefore $[NP]$ drops with the particle diameter given we intentionally standardize the total extinction of all the NPs. Clearly from the optical images (Figure 2 a-d), the color of the assay is redder for small NPs but greener for larger ones, attributed to redshift in extinction resonance wavelengths at larger NP sizes. Therefore, the NP size could affect the human eye sensitivity in colorimetric detection.

Further, we investigated the effect of NP size on the assay sensitivity (Figure 2 e-l). Visual inspection of the sample-loaded well plate by naked eye indicates a gradual supernatant color change from almost colorless at >10 nM to red at <100 pM for all sizes. Noticeably, a significant color contrast was observed in distinguishing 10 nM and higher sGP concentration from the reference negative control (NC) sample (with only PBS buffer but no sGP), indicating that

clinically relevant sGP concentrations can be readily detected by naked eyes. The naked eye diagnostics would be very useful for qualitative or semi-quantitative diagnostics in resource-limited settings, but more accurate quantification would require analysis of the optical spectra of the assay supernatants.

Here the UV-visible extinction spectra were collected for all AuNPs (Figure 2 e-h). The extinction is defined as $E = \log_{10}\left(\frac{I_0}{I}\right)$, where E is the extinction resulted from AuNP scattering and absorption, I_0 is the intensity of light passing reference cuvette and I is the intensity of light passing sample cuvette. According to Beer-Lambert law $E = \varepsilon cl$ (E extinction, ε extinction coefficient, c concentration, l optical path), the decrease of extinction indicates decreased AuNP monomer concentration in supernatant, consistent with our proposed sensing mechanism. We further extracted the extinction peak intensity for each assay sample and plotted the standard curves of extinction versus concentration for each AuNP size (Figure 2i-l). The sGP signal at low concentration (<10 pM) was indistinguishable from the NC signal (with an extinction E_{NC} within the range of 0.4-0.45). It then displayed a clearly large dynamic range of from ~100 pM to ~100 nM for all AuNP sizes, with the extinction dropped to 0.1 to 0.2, *i.e.* 60-80 % change. The extinction displayed little change for highly concentrated sGP samples (100 nM and above), indicating an upper limit in detection.

The experimentally found upper and lower limits in detection are thought to be correlated to the multivalent binding nature of the detection process. We note from suppliers that up to 120, 270, 460, and 730 streptavidin are bound on 40, 60, 80 and 100 nm diameter NPs, although the effective numbers are expected smaller. With very small amount of antigens, the ultimate lower limit of detection occurs when the NP precipitation decreases the AuNP monomers in the suspension

significant enough to produce a signal that is distinguishable from the noise or fluctuation. This value is expected dependent on both the dynamic antigen-antibody binding process and the experimental setup. For example, assuming a very high affinity in sGP binding (ignoring dissociation) and 4 sGP bound to each aggregating AuNP (about 3-5 at 1 nM from TEM image from Figure S5) and setting 3% optical extinction change as detection threshold, we could estimate the LoD as 275×(3%/45%)×4=70 pM or 36×(3%/45%)×4=10 pM for 40 and 80 nm AuNPs, which are comparable to our experimental analysis. Similarly, the upper limit of detection could be estimated when the AuNPs are completely saturated with the analyte, *e.g.* 120×0.275=33 nM and 460×0.036=16 nM for 40 and 80 nm AuNPs, also comparable to but smaller than experimental values. The above back-on-the-envelope analysis is helpful to provide intuitive understandings of the measured dynamic range and detection limits, but also quite limited because it ignores the dynamic association and dissociation processes which are thought to be dependent on both the NP size and antigen-nanobody binding characteristics.

In addition to the detection limits, the assay detection time was studied at 10 nM sGP concentration in 1× PBS (Figure S4). The extinction generally started to drop after 0.5-1.5 hour for all sizes, indicating a stage to initiate aggregate formation and precipitation. Extended incubation led to a nearly linear extinction drop, at a rate of 0.049, 0.071, 0.080, and 0.091 hr^{-1} for 40, 60, 80, and 100 nm NPs, eventually reaching a stable value after 7, 5.5, 4, and 4.5 hours. This can be understood intuitively from the impact of AuNP size and concentration on the antigen binding dynamics and the precipitation process. On one hand, smaller NPs have higher concentrations, considering the suspension extinction $\sigma_{ext} \propto [NP]d^3$ was set about the same for all sizes, and therefore are expected to initiate the antigen-binding and NP aggregation reaction relatively faster. On the other hand, the precipitation of smaller aggregates will take longer time,

resulting in a longer incubation period. These are consistent with observed from the experimental dynamic studies. Importantly, this dynamic extinction test indicated that high-contrast colorimetric detection by incubation can take a few hours, which prompted us to establish a rapid testing scheme to be discussed later.

These above analyses suggest 80 nm AuNPs as an excellent choice in detecting sGP in PBS buffer, because they show the highest sensitivity (~10 pM, compared to ~100 pM for other sizes, Figure 2), the largest detection dynamic range (up to 4 orders, compared to 2-3 orders for other sizes, Figure 2), and the shortest detection time (3-4 hours, compared to 4 to 7 hours for other sizes, Figure S4). Therefore, we decided to select 80 nm AuNPs for further studies of the sensing mechanism, sGP sensitivity/specificity test in diluted serum, as well as rapid and portable readout.

Structural characterization of Nano2RED assay in sGP sensing.

To understand the assay's working mechanism, we complemented the colloid-state testing with a variety of methods to investigate the samples in solid state. We also conducted a number of different structural and optical characterization methods, including scanning electron microscope imaging, UV-visible spectroscopy and dark field scattering imaging to inspect the drop-cast and dried samples on glass and gold substrates. First, the assay colloids at the bottom of Eppendorf tube was collected and imaged by cryogenic transmission electron microscope (CryoTEM). Cryogenic sample preparation is known to prevent water crystallization and hence preserve protein structures and protein-protein interaction. Consistent with the sensing mechanism described above, aggregates of AuNPs formed with 1 nM sGP present in the precipitates (Figure 3a) with average cluster size of 1.8 by 1.4 μm, while only 80 nm AuNP monomers but no clusters were observed in the supernatant of 1 nM sGP sample (Figure 3b) or in the precipitates of NC sample (Figure S5).

Even larger AuNP aggregates were observed at higher sGP concentration (Figure S5), but the aggregate sizes had a large distribution, probably due to random aggregation process and sample preparation, and thus not ideal to correlate with the sGP concentration.

Additionally, the 80 nm AuNP assay supernatants (1 μL, n_{AuNP} = 0.036 nM) with sGP from 1 pM to 1 μM in PBS were drop-casted on a 1 mm thick glass slide for colorimetric and spectrometric inspections (Figure 3c). It can be observed that the dried sample spots displayed light red color, and its transparency increased from around 10 nM (spot 3) and became readily differentiable by naked eye at 1 μM (spot 1) compared to reference NC sample (spot 8). We then measured the extinction spectra of each drop-cast spots and extracted the extinction peak intensity at LSPR resonance (Figure 3d and 3g). The extinction spectra featured AuNP LSPR peaks, similar to those supernatant measurement in PDMS well plate (Figure 2), but the peak intensity was about one order of magnitude smaller attributed to significantly shorter optical path (estimated ~300 μm) compared to the PDMS well plate (~3 mm). These samples were stored at room temperature (25 ˚C) over 12 weeks and re-inspected, and the optical signals were found very consistent over such an extended storage period (Figure S6). The above analysis showed the feasibility of quantitative detection of sGP down to 350 pM LoD with broad detection dynamic range (100 pM to 1 μM) using a simple and small solid-state sample carrier, offering promising solutions to simplified sample preparation and prolonged preservation that is potentially advantageous in retrospective cohort studies.

Additionally, scanning electron microscopy (SEM) was employed to investigate the AuNP aggregation in the supernatant. Here 1 μL of 80 nm AuNP assay colloids (n_{AuNP} = 0.036 nM, 1×PBS) with targeted sGP (1 pM to 1 μM) were drop-casted on an oxygen plasma treated gold surface and subsequently dried in air (Figure 3e). Gold surface was selected due to its high electron

conductivity that dramatically improves the contrast and resolution in imaging. Only AuNP monomers but no large aggregates were observed from the SEM images (Figure 3f), confirming that the majority, if not all, of the aggregates should precipitate at the bottom of the tubes. Further, the 80 nm AuNPs were recognized and counted through image analysis, and their density was statistically determined from ten SEM images (total area 10 × 8.446 × 5.913 μm^2) at each sGP concentration (Figure 3h). Clearly, the AuNP density decreased at higher sGP concentration, *e.g.*, from 1.97 μm^{-2} at about 10 pM to 0.26 μm^{-2} at 100 nM and finally saturated to 0.24 μm^{-2} at about 1 μM or above, which was in accordance with extinction spectrometric measurements of both supernatant samples (Figure 2d) and glass slide drop-cast samples (Figure 3g). The limit of detection derived from SEM characterization was estimated about 150 pM, comparable but slightly higher than colloid supernatant extinction characterization for the same 80 nm AuNPs in PBS, possibly due to increased variance in nanoscale level characterization and limited sampling data. In comparison, we also performed drop-casting of 60 nm AuNPs on glass slides (Figure S7), which also shows similar performance compared to detection in PDMS well plate (Figure 2).

Finally, the drop-cast samples on gold surface were also analyzed by dark field scattering imaging, which has been widely applied in biomolecule sensing and environmental toxin detection[32-34]. Here LSPR mediated scattering of incident light from AuNPs on gold surface can directly indicate the density of AuNP, based on the density of bright spots on dark field imaging (Figure S8). It can be observed that the density of bright spots (averaged on 10 images, captured area 62.5 μm × 62.5 μm in each image) dropped as sGP concentration increased (Figure 3i), consistent with SEM observation. The dark-field imaging method was estimated to be capable of detecting sGP with a sensitivity about 1 nM.

Besides using 80 nm AuNPs, 100 nm AuNPs were also examined under spectroscopy on a glass

slide, as well as SEM and dark field scattering imaging on a gold surface (Figure S9). The measurement results in general showed comparable sensitivity (sub 1 nM) to that of 80 nm AuNPs and consistent with detection in PDMS well plate. As demonstrated above, these solid-state characterization methods, including spectroscopy, SEM and dark field scattering imaging, provided valuable insight into the nano-scale NP aggregation process, and could serve as alternative sensing methods with sub 1 nM detection limit.

Assay performance for sGP sensing in diluted fetal bovine serum using 80 nm AuNPs

The sGP sensing sensitivity, specificity and temperature stability were analyzed in diluted fetal bovine serum (FBS, five-fold diluted by 1×PBS) using 80 nm AuNPs (Figure 4). Again, the supernatant samples after 3-hour incubation were loaded into a PDMS well plate, and measured with spectrometer (Figure 4a). The extinction peak intensity were extracted and plotted as the standard curve versus concentration (Figure 4b black data points). Compared to NC sample (E_{NC}=0.481) and low concentration (E_{1pM}=0.475), the sGP extinction signal started to display an appreciable difference from 10 pM (E_{10pM} =0.459), which significantly dropped at even higher concentration, *i.e.* E_{100pM}=0.414 and E_{100nM}=0.106. Not surprisingly, the extinction displayed little change at a concentration higher than 100 nM, very similar to the test in PBS. Clearly, this demonstrated the feasibility of our AuNP assay to detect over a broad range from 10 pM to 100 nM, which largely overlaps with the sGP concentration range possibly found in patients' blood (sub-nM to μM) attributed from patient-patient and infection stage variation[15, 35]. Here the three-sigma limit of detection (LoD), defined as the concentration displaying an extinction of $E_{NC} - 3\sigma$ where σ is the measurement variation, was found about 87 pM (9.6 ng/ml), which is 9 times more sensitive than the standard sandwich ELISA we measured using the same reagents (~0.8 nM,

Figure 4c). Both the broadband dynamic range and high sensitivity therefore indicate that our Nano2RED assay is highly feasible for precise sGP quantification and early stage EBOV infection.

Assay specificity is crucial to accurate diagnostics, because low specificity can cause false positive EVD diagnostic results and lead to unnecessary hospitalization and even serious clinical incidents such as nosocomial infection. Here we tested sGP against GP1,2, a homotrimer glycoprotein transcribed from the same GP gene and share its first 295 residues with sGP [14]. The majority of GP1,2 can be found on virus membrane whereas a small portion are released into patients' bloodstream, also known as shed GP. The close relevance of GP1,2 to sGP makes it a very strong control molecule to assess our assay's specificity. Indeed, the extinction signals of GP1,2 at different concentrations from 1 pM to 1 uM are all very similar to NC, showing only a small fluctuation. This high specificity can be attributed to minimal AuNP aggregates formation in the presence of GP1,2 (Figure 4b, red datapoint set).

We also measured the temperature stability in sGP detection from 20 to 70°C (Figure 4d), and found the 10 nM sGP can be easily distinguished from NC sample at all tested temperatures. This indicates our assay can be transported, stored and tested at ambient temperatures without serious concerns of performance degradation, which is very important for POC testing.

Rapid sGP detection.

The PDMS well plate based spectrometric measurement required 3 hours incubation time to allow effective AuNP bridging and precipitation, which is comparable to ELISA but shorter than most RT-PCR assays. However, rapid diagnostics, *e.g.* less than 30 minutes, is usually much favorable in infectious disease diagnosis and critical to mass screening and the control of disease spread. To meet this goal, we further studied the sensing mechanism and established a simple

model aimed at reducing the detection time. Using 80 nm AuNP as an example, we first attempted to identify the key rate-determining step in the sensing mechanism. Each of the 80 nm AuNPs has ~460 nanobodies on their surface, and behaves as a multivalent sGP-binding pseudo-particle that diffuses and conjugates to each other via sGP-mediated bridging. This triggers formation of AuNP dimers oligomers, and eventually large clusters, which precipitate at the bottom of centrifuge tube as the gravity gradually overtakes fluidic drag force. A comprehensive study of such complex dynamics typically requires Monte Carlo simulation and extensive experimental verification[36-38], which will be investigated in our future studies. Instead, we developed a simplified model based on Smoluchowski's coagulation equation to understand the irreversible aggregation process (Figure 5 a-b, more detailed discussion in supplementary section 5)[39]. This model estimated that the aggregation time constant τ_{agg} is 0.87 hour at 0.036 nM 80 nm AuNP assay in detection of 10 nM sGP. On the other hand, as gravitational force overcomes fluidic drag, large clusters precipitate to form sedimentation and continuously deplete AuNPs and sGP proteins in the colloid until reaching equilibrium. The sedimentation time of this progress can be estimated from the solution of Mason-Weaver equation by $\tau_{sed} = z/(s \cdot g)$ where z is precipitation path (the height of colloid liquid), g is the gravitation constant, s is the sedimentation coefficient $s = \frac{d^2}{18\eta}(\rho_M - \rho_w)$ (d is the aggregate diameter, η is the dynamic viscosity of colloid buffer, ρ_M and ρ_w are the density of aggregate and colloid buffer, respectively) [40]. Given z ~3.5 mm for 16 µL liquid in centrifuge tube, we calculated that τ_{sed} decreases from 26.0 hours for an 80 nm AuNP monomer to 1.0 and 0.3 hours for 400 nm and 800 nm diameter cluster. Taking into account both the aggregation and precipitation steps, the estimated sensing incubation time is consistent with the experimentally observed 2~3 hours.

From the above analyses, the key to reduce the assay incubation time is to decrease aggregation and precipitation time. Here, we attempted to use centrifugation to both enhance the reagents concentration and decrease the precipitation path for rapid diagnostics (Figure 5c). After mixing AuNPs with sGP antigens, an extra brief centrifugation step (3,500 rpm or 1,200 × g, 1 min) was used to concentrate AuNP monomers at the bottom of Eppendorf tube without causing dense AuNP aggregation. Optical image taken for the assay after centrifugation (Figure 5d) showed that the AuNPs were highly localized with sediment of estimated ~150 um in height formed at the bottom of the centrifuge tube, or >20 times reduction in precipitation path and accordingly τ_{sed}. Additionally, the concentrated AuNPs are confined to an estimated <0.34 μL volume, or ~50 times concentration increase from original 16 μL colloid liquid, leading to a greatly reduced aggregation time τ_{agg} estimated from 0.87 hour to 0.024 hour (Figure 5b). These calculations indicate that both the aggregation formation and precipitation of the aggregates can take place in as short as a few minutes.

To confirm the feasibility of rapid diagnostics, the assay colloid was thoroughly vortexed to resuspend free AuNP monomers after centrifugation and a 20 min incubation. This mixing step was meant to release the AuNP monomers that could have been physically adsorbed to the tube bottom. Indeed, the increased assay supernatant transparency with increasing sGP concentration (Figure 5e) was distinguished by bare eyes for the sGP concentration >1 nM. From the extinction spectra of the supernatants (Figure 5f), we extracted the extinction at its maximum value (~559 nm in wavelength) for each sGP concentration (Figure 5g). The extinction-concentration standard curve for 20-min rapid detection was consistent with the measurement for 3-hour incubation, with slightly lower limit of detection (36 pM) and comparable dynamic ranges (100 nM to 10 pM). Further applying this rapid-detection method to detect 10 nM sGP at different incubation time, we

found the color contrast was high enough to be immediately resolved by naked eye after vortex mixing, without additional incubation (Figure S11a). Further analyzing the peak extinction of the assay supernatant at different incubation time (Figure 5h), the extinction was found 0.145 right after vortex, completely distinguishable from the NC sample (0.536), and gradually decreased to 0.110 as incubation time was extended to 20 min. Including all the amount of time for sample collection, pipetting, centrifugation, vortex mixing and readout (by naked eyes), our Nano2RED assay could be completed within minutes. In addition, the rapid sGP detection scheme was found reproducible in fetal bovine serum (Figure S12 a-b) and produced similar results in 1×PBS buffer (Figure S12 c-d). In both cases, sGP >1 nM can be accurately read out with bare eyes either in tubes or in a PDMS well plate. Considering that 10 nM and higher sGP concentration is typical for EVD patients[13, 15, 35], this rapid-detection method is particularly suitable for high-speed mass screening of EVD-susceptible populations.

Point-of-care detection of sGP in fetal bovine serum.

Extinction spectrometric analysis provides quantitative and accurate diagnostics, but requires bulky spectrometer systems that are more suitable for lab use. Here we demonstrate the feasibility of detecting sGP in fetal bovine serum using a cost-efficient portable UV-visible spectrometer system towards field deployment. Additionally, we develop a homemade LED-photodiode based electronic readout system with significantly reduced system cost to deliver accurate and sensitive detection results comparable to lab-based spectrometer system.

The portable UV-visible spectrometer system (Figure S13) consists of a smartphone sized Ocean Optics UV-visible spectrometer (8.8 × 6.3 × 3.1 cm^3), a lamp source module (15.8 × 13.5 × 13.5 cm^3), alignment clamps and an electronic recording device (such as a laptop or a smart

phone). Here 80 nm AuNP colloid (30 µL) with sGP contained fetal bovine serum (10 µL), vortexed and centrifuged the assay at 1,200 × g (3,500 rpm) for 1 mins (Figure 5e). After 20 mins of incubation, the assay colloids were vortexed for 15 seconds and the supernatants were loaded into 4 mm-diameter wells on a 3 mm thick PDMS plate (Figure S12). The light from lamp source transmitted through the colloid, with the glass slide covered in black to block light transmission, and collected by the spectrometer through a fiber waveguide. The extinction spectra measured by portable spectrometer (Ocean Optics, Figure S13b) was in general highly consistent with that by microscope-coupled spectrometer (Horiba iHR320, Figure S13c), with slightly increased signal noise. The extinction peak values at the resonance wavelength (~559 nm) of the two measurements were in great agreement, with a small difference within 15.8% possibly attributed to different collection angles (10× objective, NA=0.3 collection versus waveguide collecting nearly collimated beam). The optical signals measured by portable spectrometer were able to distinguish sGP at 100 pM (E_{100pM}=0.509) from the reference (E_{NC}=0.542, no sGP), with a dynamic range (10 pM to 1 µM) and limit of detection (~42 pM) comparable to that of rapid detection of sGP in serum and 1 × PBS (Figure 5g and Figure S12).

Finally, we further simplified the measurement system by establishing an electronic signal readout system using commercially available and inexpensive electronic components (Figure 6). In this mechanism (Figure 6a), a LED light source emits narrowband wavelength light centered at the AuNP extinction peak wavelength (λ_P = 560 nm, $FWHM_P$ = 40 nm) that transmits through the assay supernatant before being measured by a photodiode. As a result, photocurrent or photovoltage are generated on a serially connected load resistor in a simple circuitry that can be easily integrated and scalably produced. In practice, we 3D printed a black part that holds the Eppendorf tube holder and mounts both the LED and photodetector (Figure 5b). LED and

photodiode were powered by AA alkaline batteries (3V and 4.5V respectively), and the bias voltages were carefully adjusted by serially connected resistors to ensure wide-range detection of sGP proteins without saturating the photodetectors. Using 80 nm AuNP assays to detect sGP in PBS diluted fetal bovine serum (five-fold diluted) and adopting the centrifuge assisted rapid diagnostics method, this portable electronic system was prototyped to read the photovoltage signals (Figure 6c, V_R) by a handheld multimeter. As a comparison, the measurement results of the same samples by lab-based spectrometer (blue datapoints) displayed the same monotonous trend and dynamic range from 10 pM to 1 μM. Our electronic readout system has significant advantages in a few aspects. First, the system cost is significantly reduced attributed to low cost of massively manufacturable electronic components, *e.g.* LED and photodiode cost less than $1 each used in our experiments and can be <$0.1 when ordered in bulk. Second, the footprint of the Nano2RED readout system can be further scaled down for POC applications by further reducing the tube holder dimensions and integrating electronic components and power supplies on a circuit board. Further, the electronic readout is potentially as accurate as the spectrometric method but much better than bare-eye readout, more accessible without color vision limitation, and more readily available for data storage in computers or online database for real-time or retrospective data analysis.

Conclusions and Outlook

In conclusion, we have demonstrated the ultrafast generation of the affinity reagent against a selected viral antigen, *e.g.* Ebola sGP protein, and standardized preparation of AuNP based Nano2RED assay for POC testing. The Nano2RED sensing mechanism is based on sGP-triggered aggregation of multivalent AuNP monomers and resultant modulation of colloid color. Using high-affinity anti-sGP nanobody sGP49 produced by phage display selection method from a well-designed high diversity synthetic combinatorial library, we show that Ebola sGP antigens can be detected after incubation for about 3 hours with a sensitivity of 10 nM by bare eyes or 81 pM spectroscopically in a customized PDMS well plate, which is ~9 times better than ELISA using the same reagents. We studied the size impact on the sensing performance, including the assay time, detection limits, and dynamic range. We further experimentally investigated different methods to study the AuNP aggregation mechanism by analyzing dried samples with optical spectroscopy, electron microscopy, and dark-field imaging, and coupled with theoretical analysis using a modified Smoluchowski's coagulation. Such understandings allowed us to develop a rapid diagnostics strategy to detect sGP at 10 nM and above with minimal incubation and at ~10 pM with less than 20 min incubation by introducing a simple centrifugation step that concentrates the AuNPs and shortens their precipitation paths. Additionally, we prototyped a miniaturized spectrometer and a compact and low-cost electronic readout system for portable diagnostics, and achieved a sensitivity and dynamic range comparable to lab-based spectrometer measurement. This study proves that the Nano2RED assay has all the potentials as a portable, rapid, accurate, and low-cost method for POC diagnostics and mass screening of early stage Ebola virus infection, particularly in resource-limited regions. This design may also inspire applications to other infectious diseases, such as influenza and coronavirus disease 2019 (COVID-19).

METHODS

Materials. Phosphate-buffered saline (PBS) was purchase from Fisher Scientific. Bovine serum albumin (BSA) and molecular biology grade glycerol and were purchased from Sigma-Aldrich. Fetal bovine serum (FBS) was purchased from Gibco, Fisher Scientific. FBS was avoided heat inactivation to best reflect the state of serum collected in field. Poly(vinyl alcohol) (PVA, Mw 9,000-10,000) was purchased from Sigma-Aldrich. Sylgard 184 silicone elastomer kit was purchased from Dow Chemical. DNase/RNase-free distilled water used in experiments was purchased from Fisher Scientific. Phosphate Buffered Saline with Tween 20 (PBST), Nunc MaxiSorp 96 well ELISA plate, streptavidin, 1% casein, 1-Step Ultra TMB ELISA substrate solution, isopropyl-β-D-galactopyranoside (IPTG) were purchased from Thermo Fisher Scientific. HRP-M13 major coat protein antibody was purchased from Santa Cruz Biotechnology. Sucrose and imidazole were purchased from Sigma-Aldrich. 5 mL HisTrap column, HiLoad 16/600 Superdex 200 pg column, HiPrep 26/10 desalting column were purchased from GE Healthcare. BirA using a BirA-500 kit was purchased from Avidity. Streptavidin (SA) Biosensors were purchased from ForteBio. The streptavidin surface functioned gold nanoparticles were purchased from Cytodignostics, dispersed in 20% v/v glycerol and 1 wt% BSA buffer. Thiolated carboxyl poly(ethylene glycol) linker was self-assembled on AuNP through thiol-sulfide reaction. Streptavidin was then surface functioned through amine-carboxyl coupling by N-Hydroxysuccinimide/1-Ethyl-3-(3-dimethylaminopropyl)carbodiimide (NHS/EDC) chemistry.

Phage display selection. sGP protein binder selection was done according to previously established protocols[21]. In brief, screening was performed using biotin and biotinylated-sGP protein-bound streptavidin magnetic beads for negative and positive selections, respectively. Prior

to each round, the phage-displayed nanobody library was incubated with the biotin-bound beads for 1 h at room temperature to remove off-target binders. Subsequently, the supernatant was collected and incubated with biotinylated-sGP protein-bound beads for 1 h. Beads were washed with 10× 0.05 % PBST (1×PBS with 0.05% v/v Tween 20) and phage particles were eluted with 100 mM triethylamine. A total of three rounds biopanning were performed with decreasing amounts of antigen (200 nM, 100 nM, 20 nM). Single colonies were picked and validated by phage ELISA followed by DNA sequencing.

Single phage ELISA. ELISAs were performed according to standard protocols[21]. Briefly, 96 well ELISA plates (Nunc MaxiSorp, Thermo Fisher Scientific) were coated with 100 µL 5 µg/mL streptavidin in coating buffer (100 mM carbonate buffer, pH 8.6) at 4˚C overnight. After washing by 3× 0.05 % PBST (1×PBS with 0.05% v/v Tween 20), each well was added with 100 µL 200 nM biotinlyated sGP protein and incubated at room temperature for 1 h. Each well was washed by 5× 0.05 % PBST, blocked by 1% casein in 1×PBS, and added with 100 µL single phage supernatants. After 1 h, wells were washed by 10×0.05% PBST, added with 100 µL HRP-M13 major coat protein antibody (RL-ph1, Santa Cruz Biotechnology; 1:10,000 dilution with 1×PBS with 1% casein), and incubated at room temperature for 1 h. A colorimetric detection was performed using a 1-Step Ultra TMB ELISA substrate solution (Thermo Fisher Scientific) and OD450 was measured with a SpectraMax Plus 384 microplate reader (Molecular Devices).

sGP49 purification and biotinlyation. sGP49 was expressed as a C-terminal Avi-tagged and His-tagged form in E. coli and purified by Ni-affinity and size-exclusion chromatography. In brief, E. coli strain WK6 was transformed and grown in TB medium at 37˚C to an OD600 of ~0.7, then induced with 1 mM isopropyl-β-D-galactopyranoside (IPTG) at 28˚C for overnight. Cell pellets were resuspended in 15 mL ice-cold TES buffer (0.2 M Tris-HCl pH 8.0, 0.5 mM EDTA, 0.5 M

sucrose) and incubated with gently shaking on ice for 1 h, then added 30 mL of TES/4 buffer (1:4 dilution of the TES buffer in ddH_2O) and gently shaken on ice for 45 min. Cell debris was removed by centrifugation at 15,000×g, 4˚C for 30 mins. The supernatant was loaded onto a 5 mL HisTrap column (GE Healthcare) pre-equilibrated with the lysis buffer (50 mM sodium phosphate, pH 8.0, 300 mM NaCl, 10 mM imidazole, 10% glycerol). The column was washed with a washing buffer (50 mM sodium phosphate, pH 8.0, 300 mM NaCl, 20 mM imidazole, 10% glycerol) and then His-tagged proteins were eluted with an elution buffer (50 mM sodium phosphate, pH 8.0, 300 mM NaCl, 250 mM imidazole, 10% glycerol). Eluates were loaded onto a HiLoad 16/600 Superdex 200 pg column (GE Healthcare) pre-equilibrated with a storage buffer (1×PBS, 5% glycerol). Eluted proteins were concentrated, examined by SDS-PAGE, and quantified by a Bradford assay (BioRad), then flash frozen in 100 µL aliquots by liquid N_2 and stored at -80˚C.

The purified sGP49 was biotinylated by BirA using a BirA-500 kit (Avidity). Typically, 100 µL BiomixA, 100 µL BiomixB, 4 µL 1 mg/mL BirA, were added to 500 µL ~1 mg/mL sGP 49 to a final volume of 1000 µL. The biotinylation mixture was incubated at room temperature for 1 h and then loaded onto a HiPrep 26/10 desalting column (GE Healthcare) pre-equilibrated with a storage buffer (1×PBS, 5% glycerol) to remove the free biotin.

Binding kinetics analysis. sGP49 binding kinetics was analyzed using an Octet RED96 system (ForteBio) and Streptavidin (SA) biosensors. 200 nM biotinylated sGP target protein was immobilized on SA biosensors with a binding assay buffer (1×PBS, pH 7.4, 0.05% Tween 20, 0.2% BSA). Serial dilutions of sGP 49 was used for the binding assay. Dissociation constants (K_D) and kinetic parameters (k_{on} and k_{off}) were calculated based on global fit using Octet data analysis software 9.0.

Preparation of sGP49 surface functioned AuNP colloid. The streptavidin surface functioned

gold nanoparticles (0.13 nM, 80 μL) were first mixed with excessive amount of biotinylated sGP49 nanobody (1.2 μM, 25 μL). The mixture was then incubated for 2 hours to ensure complete streptavidin-biotin conjugation. Next, the mixture was purified by centrifuge (accuSpin Micro 17, Thermo Fisher) at 10,000 rpm for 10 mins and repeated twice to remove unbounded biotinylated sGP49 nanobody. The purified AuNP colloid was measured by Nanodrop 2000 (Thermo Fisher) to determine the final concentration. The concentration of AuNP in colloid was subsequently adjusted to 0.048 nM and was aliquoted into 12 uL in a 500 uL Eppendorf tube. sGP stock solution (6 μM, in 1×PBS) underwent 10-fold serial dilution and 4 uL sGP solution of each concentration (4 pM to 4 uM) was mixed with 12 uL AuNP assay colloid and briefly vortexed (mini vortexer, Thermo Fisher) at 800 rpm for 5 seconds. The buffer used in assay preparation and sGP dilution was prepared by diluting 10×PBS buffer and mixing with glycerol and BSA to reach final concentration of 1×PBS, 20% v/v glycerol and 1 wt% BSA.

Centrifuge enhanced rapid detection method. Same protocols were followed in preparation of sGP49 surface functioned AuNP colloid. After mixing sGP49 surface functioned AuNP colloid with sGP solution, AuNP assay colloid was centrifuged (accuSpin Micro 17, Thermo Fisher) at 3,500 rpm (1,200×g) for 1 minute. AuNPs were highly concentrated the bottom of Eppendorf tube. After 20 minutes of incubation, the assay colloid was vortexed (mini vortexer, Thermo Fisher) at 800 rpm for 15 seconds to thoroughly remix free AuNP monomers into colloid.

PDMS template fabrication. Sylgard 184 silicone elastomer base (consisting of dimethyl vinyl-terminated dimethyl siloxane, dimethyl vinylated and trimethylated silica) was thoroughly mixed with curing agent (mass ratio 10:1) for 30 minutes and placed in a vacuum container for 2 hours to remove the bubbles generated during mixture. The mixture was then poured into a flat plastic container at room temperature and incubated for one week until the PDMS is fully cured. The

PDMS membrane was then cut to rectangular shape and wells were drilled by PDMS puncher to form sample cuvette. 2 mm diameter wells were drilled for Olympus BX53 microscope characterization using 50×objective lens. 4 mm diameter wells were drilled for Oceanview spectrometer characterization and Olympus BX53 microscope using 10×objective lens. To prevent non-specific bonding of proteins on PDMS membrane surface, the PDMS surface was treated with PVA, adapted from methods described by Trantidou et al.[41] The as-prepared PDMS membrane and a diced rectangle shaped fused silica (500 μm thick) was rinsed with isopropyl alcohol and oxygen plasma treated at a flow rate of 2 sccm and power of 75 W for 5 min. Immediately after oxygen plasma, the PDMS membrane was bonded to fused silica to form a PDMS well plate that can load assay colloids into the wells. The PDMS plate was further oxygen plasma treated at a flow rate of 2 sccm and power of 75 W for 5 min and immediately soaked in 1% wt. PVA in water solution for 10 mins. The PDMS template was subsequently nitrogen blow dried and heated on a 110 ºC hotplate for 15 mins. Finally, the PDMS template was removed from hotplate, nitrogen blow cooled and ready to use in UV-visible spectra characterizations.

UV-visible spectra, SEM imaging and dark field scattering imaging characterizations. The UV-visible spectra were measured from a customized optical system. An Olympus BX53 microscope equipped with a LED light source (True Color, Olympus) was used to collect light signal from sample area. The PDMS template loaded colloid samples were placed on the microscope sample stage and light transmitted through AuNP assay was collected by a 50×objective lens (NA=0.8). For drop-cast samples on a glass slide, a 10×objective lens (NA=0.3) was used. The spectra were measured by a microscope-coupled UV-Vis-NIR spectrometer (iHR 320, Horiba) equipped with a CCD detector. The signal was scanned from 350 nm to 800 nm with integration time of 0.01 s and averaged for 64 times.

The SEM image was taken by Hitachi S4700 field emission scanning electron microscope at 5 kV acceleration voltage and magnification of 15,000. For each drop-cast sample spot, ten images from different regions in the spot were taken. The size of the region taken in each SEM image is 8.446 μm×5.913 μm.

The dark field scattering image was taken by Olympus BX53 microscope using an EMCCD camera (iXon Ultra, Andor). A xeon lamp (PowerArc, Horiba) was used as illumination light source. The light reflected from drop-cast samples were collected by a 100×dark field lens (NA=0.9). The integration time was set to 50 ms. For each drop-cast sample spot, ten images from different areas in the spot were taken. The size for the area taken in each dark field scattering image is 62.5 μm×62.5 μm.

Characterization of sGP in diluted fetal bovine serum. Fetal bovine serum was pre-diluted five-fold by 1×PBS buffer to minimize serum matrix effect. sGP solution (6 μM, in 1×PBS) was diluted in series and added to diluted fetal bovine serum to make sGP in serum with concentration from 4 pM to 4 uM. 30 uL 0.048 nM sGP49 surface functioned 80 nm AuNP colloid was then mixed with 10 uL sGP in serum and thoroughly vortexed. The mixture was then centrifuged following the protocol described in centrifuge enhanced rapid detection method. The incubation time for AuNP crosslinking was 20 minutes. Next, ~22 μL assay colloids detecting different sGP concentrations were loaded into 4 mm diameter wells on a 3 mm thick PDMS well plate and characterized by Horiba iHR 320 UV-visible spectrometer. A 10 × objective lens (NA=0.3) in Olympus BX53 microscope was used to collect the signal. The signals were averagely scanned from 350 nm to 800 nm for 64 times with integration time of 0.01 s.

For point-of-care demonstration, the assay colloids were initially characterized by a miniaturized portable UV-visible spectra measurement system. OSL2 fiber coupled illuminator

(Thorlabs) was used as light source. The light passed through the 4 mm diameter wells loaded with assay colloid and coupled to Flame UV-visible miniaturized spectrometer (Ocean optics) for extinction spectra measurement. The signals were averagely scanned from 430 nm to 1100 nm for 6 times and integrated for 5 seconds in each scan.

In the next step, a LED-photodiode electronic readout system was devised and demonstrated for sGP sensing with significantly reduced equipment cost. The system consists of three components: The LED light source, photodiode and centrifuge tube holder. The centrifuge tube holder was 3D printed using ABSplus P430 thermoplastic. An 8.6 mm diameter recess was designed to snug fit a standard 0.5 mL Eppendorf tube. A 2.8 mm diameter channel was open inside the centrifuge tube holder and aligned to LED, assay colloid and photodiode, forming an optical path for signal measurement. LED (597-3311-407NF, Dialight) was driven by 2 Duracell optimum AA batteries (3 V) and a 35 Ω resistor was serially connected as a voltage divider to set LED operating point. Photodiode (SFH 2270R, Osram Opto Semiconductors) was reversely biased by 3 Duracell optimum AA batteries (4.5 V) and serially connected to a 7 MΩ load resistor. The photocurrent that responds to intensity of light transmitted through the assay was converted to voltage through the 7 MΩ load resistor and measured by a portable multimeter (AstroAI AM33D).

CryoTEM sample preparation and imaging. To image AuNP precipitates, the supernatant was removed from the tube and 2~3 μL of AuNP sample colloid containing AuNP precipitates were left in the tube. The tube was then vortexed thoroughly. 2 uL of samples were pipetted and coated on both sides of an oxygen plasma treated Cu grid (Electron Microscopy Sciences, C flat, hole size 1.2 μm, hole spacing 1.3 μm). The oxygen plasma treatment time was 30 seconds. The Cu grid was plunge frozen in ethane using Vitrobot plunge freezer (FEI). The blot time was set to 6 seconds. After plunging, the sample was soaked in liquid nitrogen for long-term storage. For CryoTEM

imaging, FEI Tecnai F20 transmission electron microscope (200 kV accelerating voltage) was used. 25 high-resolution TEM images were taken for 1 μM, 1 nM sGP in PBS samples and reference sample respectively. The size of the area taken in each image is 4.476 μm×4.476 μm.

Sandwich ELISA-like assay to determine sGP detection sensitivity. In order to determine the detection sensitivity of sGP, serial dilutions of sGP protein was used for the sandwich ELISA-like assay. Briefly, 96 well ELISA plates (Nunc MaxiSorp, Thermo Fisher Scientific) were coated with 100 μL 5 μg/mL streptavidin in coating buffer (100 mM carbonate buffer, pH 8.6) at 4˚C overnight. After washing with 3× 0.05 % PBST (1×PBS with 0.05% v/v Tween 20), each well was added with 100 μL 200 nM biotinlyated sGP-49 (~100 nM) protein and incubated at room temperature for 1 h, then washed by 5× 0.05 % PBST and added with 100 μL serial dilutions (0 to 500 nM) of sGP protein and incubated at room temperature for 1 h. Each well was subsequently blocked by 1% casein in 1×PBS for 1 h, then added with 100 μL sGP 49-Phage supernatants. After 1 h, wells were washed by 10× 0.05% PBST, added with 100 μL HRP-M13 major coat protein antibody (RL-ph1, Santa Cruz Biotechnology; 1:10,000 dilution with 1×PBS with 1% casein), and incubated at room temperature for 1 h. A colorimetric detection was performed using a 1-Step Ultra TMB ELISA substrate solution (Thermo Fisher Scientific) and OD450 was measured with a SpectraMax Plus 384 microplate reader (Molecular Devices). Limit of Detection (LoD) was calculated by mean blank + 3 × SDblank.

Supporting Information

Further information on the influence of gold nano particles, vertical structure coupling, the baseline correction method, fingerprint data process.

ACKNOWLEDGEMENTS

This work is supported by a grant from the U.S. National Institutes of Health (1R35GM128918) to L. Gu. C. Wang, X. Chen, J. Zuo, and Md Ashif Ikbal acknowledge partial support from National Science Foundation under grant no. 1809997, 1838443, 1847324, 2020464, and 2027215. The samples were characterized in the Eyring Materials Center (EMC) at Arizona State University. Access to the EMC was supported, in part, by NSF grant no. 1542160. We thank D. Baker and L. Stewart for providing recombinant sGP and GP1,2 proteins and D. Williams for cryoTEM inspections.

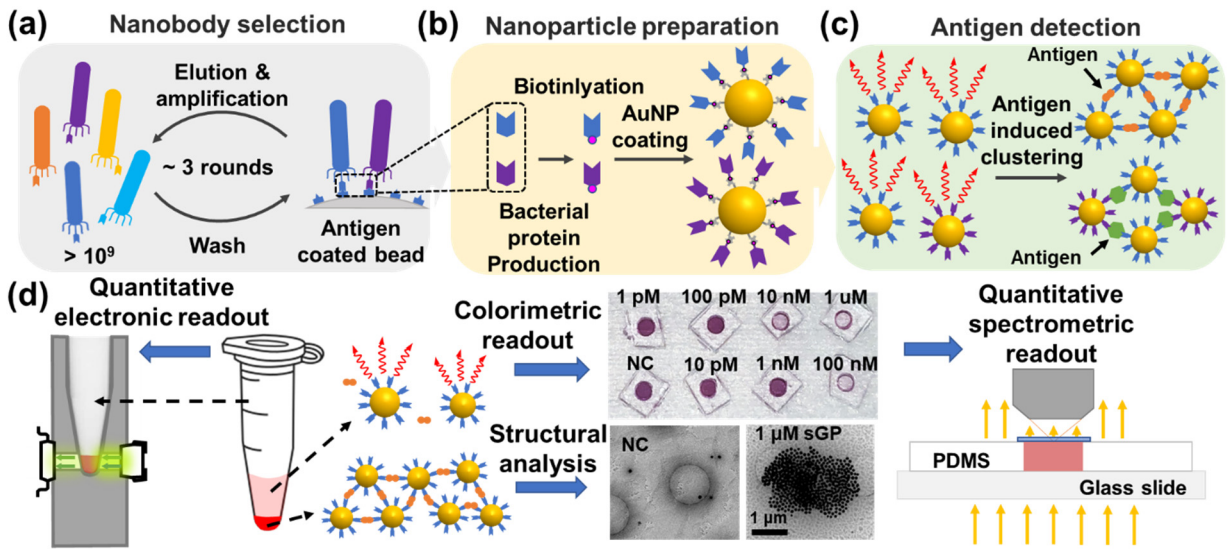

Figure 1 Nano2RED assay development and characterizations. (a)-(c) Key steps of nanobody selection and surface function of nanobody on AuNPs. (d) Schematics showing different characterization and readout methods for understanding the assay mechanism, colorimetric and quantitative determination of antigen concentration.

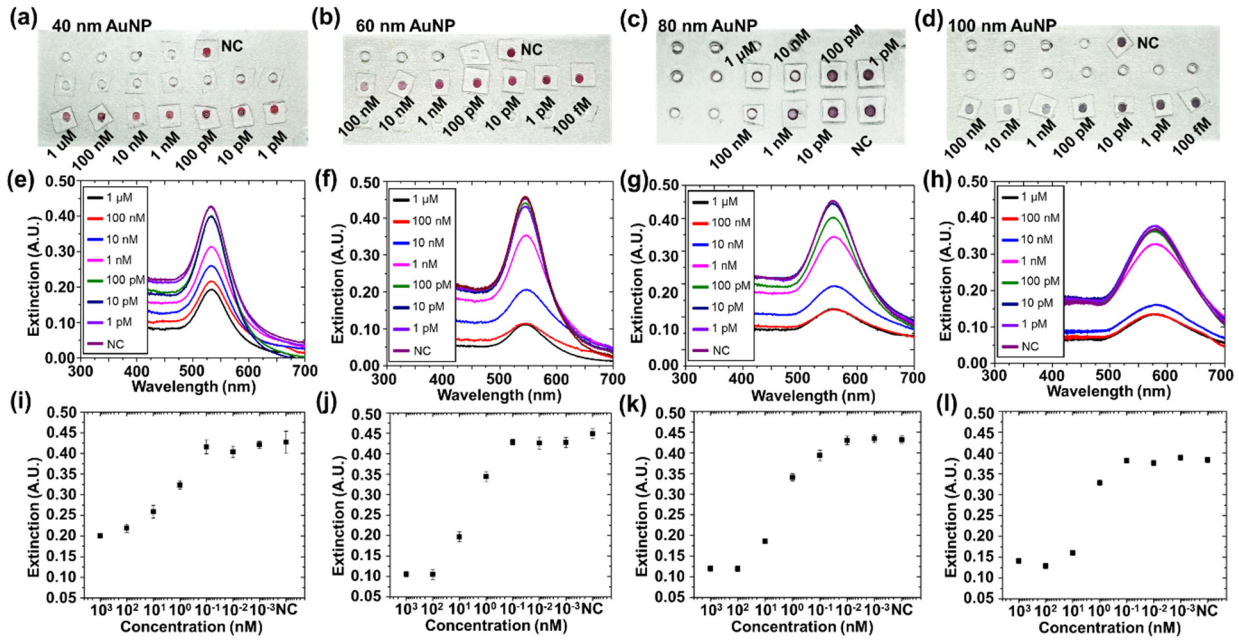

Figure 2 Study of the impact of nanoparticle size on sGP sensing performance in 1 × PBS buffer. (a)-(d) Visual image of 40, 60, 80 and 100 nm AuNP assay supernatant samples loaded on a PDMS well plate, 8, 4, 3 and 3 hours after AuNP assay mixing with 1 pM to 1 μM sGP in 1 × PBS, respectively. Concentrations were assigned in logarithmic scale. (e)-(h) Extinction spectra of samples shown in (a)-(d) panel, measured by lab-based UV-visible spectrometer system. (i)-(l) Extinction maximum plot for AuNP assay of different nanoparticle sizes in detecting sGP with concentration from 1 pM to 1 μM. Extinction maxima are derived from spectra in (e)-(h), respectively. Negative control (no sGP) is labeled as NC in all the panels.

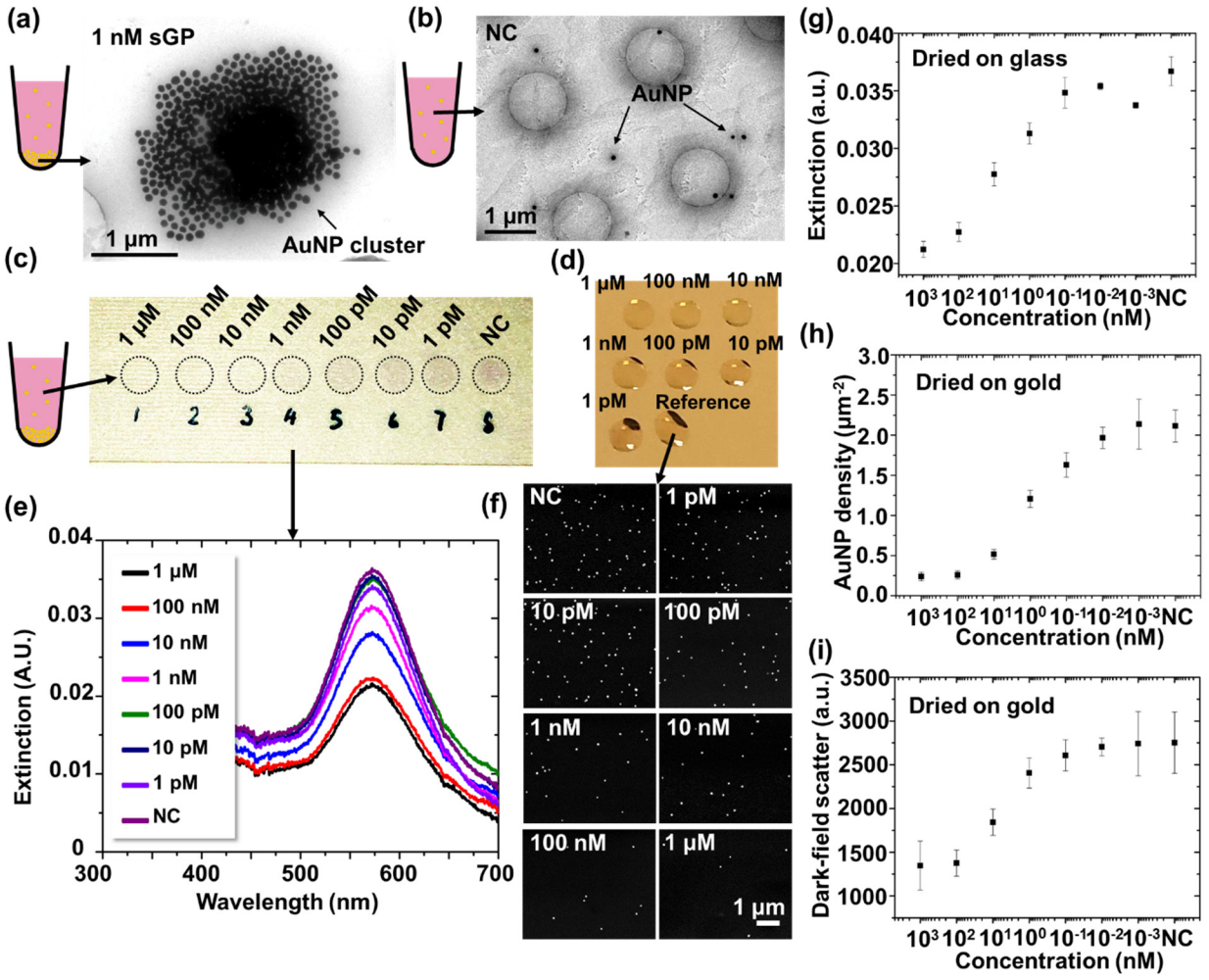

Figure 3 Structural characterization of AuNP assay in Ebola sGP sensing on a solid support. (a) Cryo-TEM image of a representative cluster in the precipitates of 80 nm AuNP assay in detecting 1 nM sGP in 1 × PBS. (b) Cryo-TEM image of 80 nm AuNPs in the negative control assay colloid. (c) Visual images of 80 nm AuNP colloid assay supernatants (sGP concentration 1 pM to 1 μM in logarithmic scale) drop-cast on a 1 mm thick glass slide. (d) Extinction spectra of 80 nm AuNP colloid assay supernatants drop-cast samples shown in (c), measured by UV-visible spectrometer. (e) Visual images of 80 nm AuNP colloid assay supernatants drop-cast on a 100 nm gold film thermally evaporated on a silicon substrate. (f) SEM image of drop-cast samples on gold

film shown in (e). (g) Extinction maximum derived from spectra in (e) at 573 nm AuNP resonance wavelength. Negative control (no sGP) is labeled as NC for comparison. (h) 80 nm AuNP density derived from SEM images taken for drop-cast samples in (d). (i) Number of AuNP dark-field scatters, shown as the bright spots in dark field scattering images taken for drop-cast samples in (d).

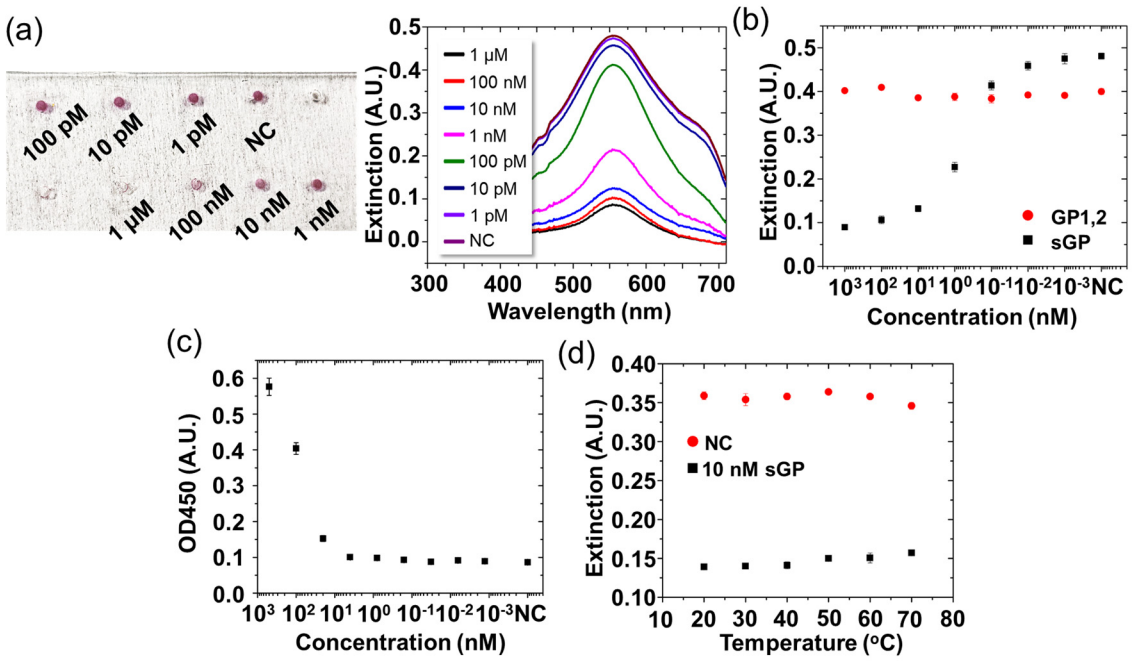

Figure 4 Spectrometric detection of sGP in 5% FBS using 80 nm AuNP colloid-based colorimetric assay. (a) Left: visual image of 80 nm AuNP assay supernatant samples loaded on a PDMS well plate, 3 hours after AuNP assay mixing with 1 pM to 1 µM sGP in 5% FBS. Concentrations were assigned in logarithmic scale. Right: extinction spectra of samples loaded on PDMS well plate, measured by UV-visible spectrometer. (b) Extinction maximum plot for AuNP assay in detecting sGP and GP1,2 with concentration from 1 pM to 1 µM. Extinction maximum is derived from spectra at 559 nm AuNP LSPR resonance wavelength. Negative control (no sGP or GP1,2) is labeled as NC in (b) for comparison. (c) Optical signals (optical density at 450 nm) measured in sandwich ELISA detection of sGP. (d) Extinction maximum plot for AuNP assay in detecting 10 nM sGP and NC at temperatures ranging from 20 ºC to 70 ºC.

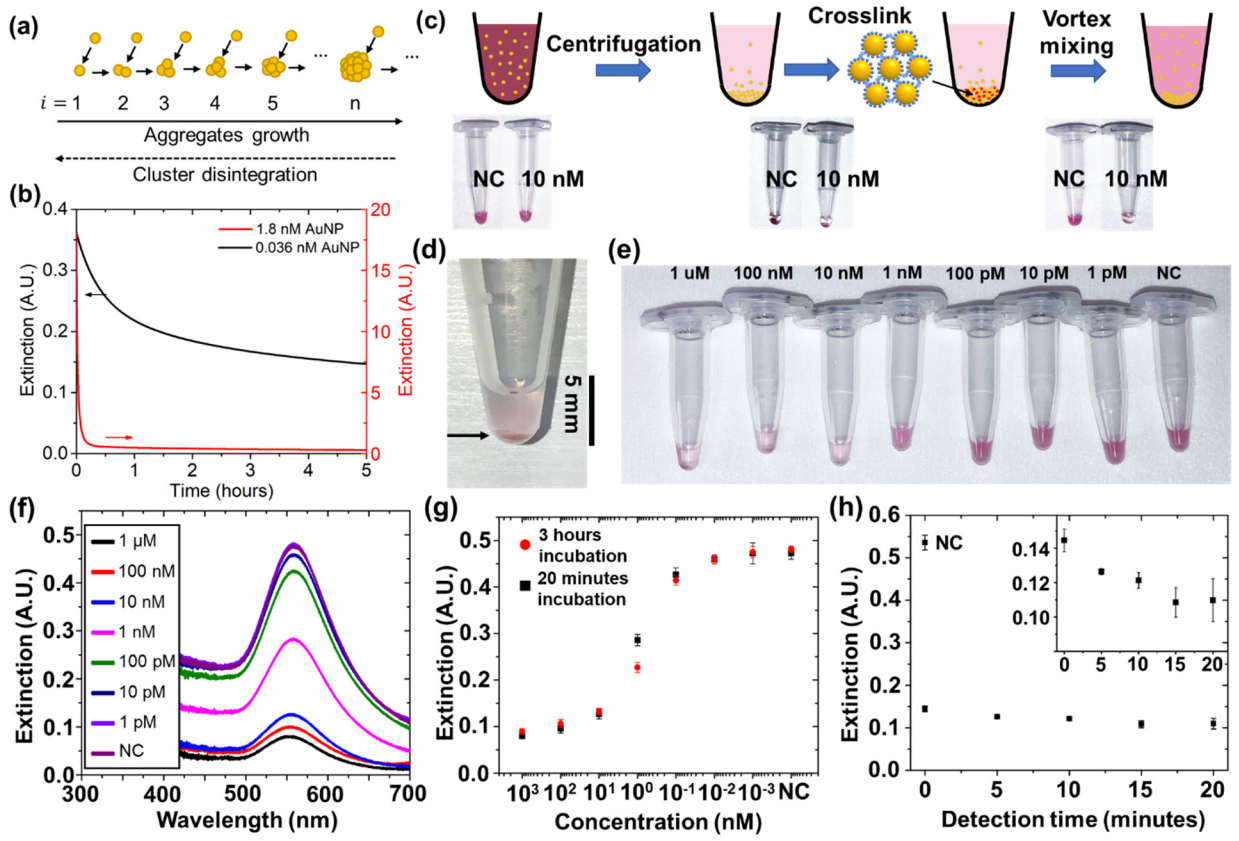

Figure 5 Rapid detection of sGP in 5% FBS using 80 nm AuNP colloid assay. (a) Modeling of aggregation formation by considering only monomer-oligomer interactions. (b) Time-dependent extinction calculated for 0.036 nM (black, as used in our experiments) and 1.8 nM (red, 50× concentrated) 80 nm AuNP assay in detecting 10 nM sGP using our model. (c) Schematic showing key steps in rapid detection protocol: centrifugation, AuNP aggregation through incubation and suspending the assay by vortex-mixing. (d) Visual image of a 0.036 nM 80 nm AuNP assay after being centrifuged at 3,500 rpm for 1 minute. (e) Visual image of Eppendorf tubes containing 80 nm AuNP colloid assay in detecting 1pM to 1 μM sGP in 5% FBS. The assays were centrifuged at 3,500 rpm for 1 minute and thoroughly vortex-mixed for 15 seconds. (f) Extinction spectra of AuNP assay shown in (e), measured by UV-visible spectrometer. (g) Extinction maximum plot for AuNP assay in rapid detection of sGP, derived from spectra in (f) at AuNP resonance wavelength

(559 nm). Measurement results of 3 hours incubation are plotted in red datapoint set for comparison. (h) Effect of incubation time on the extinction measured for samples in detecting 10 nM sGP in 1 × PBS. Inset shows narrowed extinction range for visual contrast.

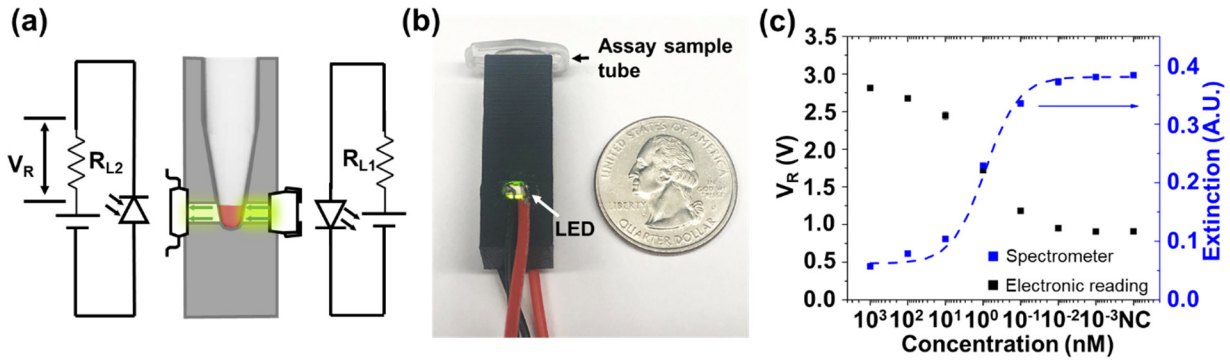

Figure 6 Point-of-care demonstration of detecting sGP in 5% FBS using miniaturized measurement system. Schematic (a) and visual image (b) of electronic readout system, consisting mainly of a LED circuit, a photodiode circuit and a 3D printed Eppendorf tube holder. (c) Voltage signals measured in detecting sGP in 5% FBS, shown as black datapoints. Lab-based UV-visible spectrometer measured extinctions for the same assays are plotted in blue datapoints.

REFERENCES

1. Couturier, C.; Wada, A.; Louis, K.; Mistretta, M.; Beitz, B.; Povogui, M.; Ripaux, M.; Mignon, C.; Werle, B.; Lugari, A., et al. Characterization and analytical validation of a new antigenic rapid diagnostic test for Ebola virus disease detection. *PLOS Neglected Tropical Diseases* **2020,** *14*, e0007965.
2. Hoenen, T.; Groseth, A.; Falzarano, D.; Feldmann, H. Ebola virus: unravelling pathogenesis to combat a deadly disease. *Trends in molecular medicine* **2006,** *12*, 206-215.
3. Worldometer COVID-19 coronavirus pandemic. **2020,** https://www.worldometers.info/coronavirus/ (Accessed
4. Perkins, M. D.; Dye, C.; Balasegaram, M.; Bréchot, C.; Mombouli, J.-V.; Røttingen, J.-A.; Tanner, M.; Boehme, C. C. Diagnostic preparedness for infectious disease outbreaks. *The Lancet* **2017,** *390*, 2211-2214.
5. Tang, Y.-W.; Schmitz, J. E.; Persing, D. H.; Stratton, C. W. Laboratory Diagnosis of COVID-19: Current Issues and Challenges. *Journal of Clinical Microbiology* **2020,** *58*, e00512-00520.
6. Kellner, M. J.; Koob, J. G.; Gootenberg, J. S.; Abudayyeh, O. O.; Zhang, F. SHERLOCK: nucleic acid detection with CRISPR nucleases. *Nature protocols* **2019,** *14*, 2986-3012.
7. Joung, J.; Ladha, A.; Saito, M.; Kim, N.-G.; Woolley, A. E.; Segel, M.; Barretto, R. P. J.; Ranu, A.; Macrae, R. K.; Faure, G., et al. Detection of SARS-CoV-2 with SHERLOCK One-Pot Testing. *New England Journal of Medicine* **2020,** *383*, 1492-1494.
8. Mina, M. J.; Parker, R.; Larremore, D. B. Rethinking Covid-19 test sensitivity—A strategy for containment. *New England Journal of Medicine* **2020,** *383*, e120.
9. Broadhurst, M. J.; Brooks, T. J. G.; Pollock, N. R. Diagnosis of Ebola Virus Disease: Past, Present, and Future. *Clinical Microbiology Reviews* **2016,** *29*, 773-793.
10. Albert, E.; Torres, I.; Bueno, F.; Huntley, D.; Molla, E.; Fernández-Fuentes, M. Á.; Martínez, M.; Poujois, S.; Forqué, L.; Valdivia, A. Field evaluation of a rapid antigen test (Panbio™ COVID-19 Ag Rapid Test Device) for COVID-19 diagnosis in primary healthcare centres. *Clinical Microbiology and Infection* **2020**.
11. Perkins, M. D.; Kessel, M. What Ebola tells us about outbreak diagnostic readiness. *Nature biotechnology* **2015,** *33*, 464-469.
12. Lisboa Bastos, M.; Tavaziva, G.; Abidi, S. K.; Campbell, J. R.; Haraoui, L.-P.; Johnston, J. C.; Lan, Z.; Law, S.; MacLean, E.; Trajman, A., et al. Diagnostic accuracy of serological tests for covid-19: systematic review and meta-analysis. *BMJ* **2020,** *370*, m2516.
13. Shubham, S.; Hoinka, J.; Banerjee, S.; Swanson, E.; Dillard, J. A.; Lennemann, N. J.; Przytycka, T. M.; Maury, W.; Nilsen-Hamilton, M. A 2′ FY-RNA motif defines an aptamer for Ebolavirus secreted protein. *Scientific reports* **2018,** *8*, 1-11.
14. de La Vega, M.-A.; Wong, G.; Kobinger, G. P.; Qiu, X. The multiple roles of sGP in Ebola pathogenesis. *Viral immunology* **2015,** *28*, 3-9.
15. Escudero-Pérez, B.; Volchkova, V. A.; Dolnik, O.; Lawrence, P.; Volchkov, V. E. Shed GP of Ebola virus triggers immune activation and increased vascular permeability. *PLoS pathogens* **2014,** *10*.
16. Maruyama, T.; Rodriguez, L. L.; Jahrling, P. B.; Sanchez, A.; Khan, A. S.; Nichol, S. T.; Peters, C.; Parren, P. W.; Burton, D. R. Ebola virus can be effectively neutralized by antibody produced in natural human infection. *Journal of virology* **1999,** *73*, 6024-6030.

17. Dolnik, O.; Volchkova, V.; Garten, W.; Carbonnelle, C.; Becker, S.; Kahnt, J.; Ströher, U.; Klenk, H. D.; Volchkov, V. Ectodomain shedding of the glycoprotein GP of Ebola virus. *The EMBO journal* **2004,** *23*, 2175-2184.
18. Brangel, P.; Sobarzo, A.; Parolo, C.; Miller, B. S.; Howes, P. D.; Gelkop, S.; Lutwama, J. J.; Dye, J. M.; McKendry, R. A.; Lobel, L. A serological point-of-care test for the detection of IgG antibodies against Ebola virus in human survivors. *ACS nano* **2018,** *12*, 63-73.
19. Wonderly, B.; Jones, S.; Gatton, M. L.; Barber, J.; Killip, M.; Hudson, C.; Carter, L.; Brooks, T.; Simpson, A. J.; Semper, A. Comparative performance of four rapid Ebola antigen-detection lateral flow immunoassays during the 2014-2016 Ebola epidemic in West Africa. *PloS one* **2019,** *14*.
20. Muyldermans, S. Nanobodies: natural single-domain antibodies. *Annual review of biochemistry* **2013,** *82*, 775-797.
21. Kang, S.; Davidsen, K.; Gomez-Castillo, L.; Jiang, H.; Fu, X.; Li, Z.; Liang, Y.; Jahn, M.; Moussa, M.; DiMaio, F. COMBINES-CID: An efficient method for de novo engineering of highly specific chemically induced protein dimerization systems. *Journal of the American Chemical Society* **2019,** *141*, 10948-10952.
22. Kaushik, A.; Tiwari, S.; Jayant, R. D.; Marty, A.; Nair, M. Towards detection and diagnosis of Ebola virus disease at point-of-care. *Biosensors and Bioelectronics* **2016,** *75*, 254-272.
23. Fontes, C. M.; Lipes, B. D.; Liu, J.; Agans, K. N.; Yan, A.; Shi, P.; Cruz, D. F.; Kelly, G.; Luginbuhl, K. M.; Joh, D. Y. Ultrasensitive point-of-care immunoassay for secreted glycoprotein detects Ebola infection earlier than PCR. *Science translational medicine* **2021,** *13*.
24. Kim, S.; Lee, J.; Lee, S. J.; Lee, H. J. Ultra-sensitive detection of IgE using biofunctionalized nanoparticle-enhanced SPR. *Talanta* **2010,** *81*, 1755-1759.
25. Zang, F.; Su, Z.; Zhou, L.; Konduru, K.; Kaplan, G.; Chou, S. Y. Ultrasensitive Ebola virus antigen sensing via 3d nanoantenna arrays. *Advanced Materials* **2019,** *31*, 1902331.
26. Huang, Y.; Chen, J.; Shi, M.; Zhao, S.; Chen, Z.-F.; Liang, H. A gold nanoparticle-enhanced fluorescence polarization biosensor for amplified detection of T4 polynucleotide kinase activity and inhibition. *Journal of materials chemistry B* **2013,** *1*, 2018-2021.
27. Zhang, L.; Salmain, M.; Liedberg, B.; Boujday, S. Naked Eye Immunosensing of Food Biotoxins Using Gold Nanoparticle-Antibody Bioconjugates. *ACS Applied Nano Materials* **2019,** *2*, 4150-4158.
28. Zhou, X.; Yang, C.-T.; Xu, Q.; Lou, Z.; Xu, Z.; Thierry, B.; Gu, N. Gold Nanoparticle Probe-Assisted Antigen-Counting Chip Using SEM. *ACS applied materials & interfaces* **2019,** *11*, 6769-6776.
29. Eustis, S.; El-Sayed, M. A. Why gold nanoparticles are more precious than pretty gold: noble metal surface plasmon resonance and its enhancement of the radiative and nonradiative properties of nanocrystals of different shapes. *Chemical society reviews* **2006,** *35*, 209-217.
30. Doyen, M.; Bartik, K.; Bruylants, G. UV–Vis and NMR study of the formation of gold nanoparticles by citrate reduction: Observation of gold–citrate aggregates. *Journal of colloid and interface science* **2013,** *399*, 1-5.
31. Link, S.; El-Sayed, M. A., Spectral properties and relaxation dynamics of surface plasmon electronic oscillations in gold and silver nanodots and nanorods. In ACS Publications: 1999.
32. Song, H. D.; Choi, I.; Lee, S.; Yang, Y. I.; Kang, T.; Yi, J. On-chip colorimetric detection of Cu2+ ions via density-controlled plasmonic core–satellites nanoassembly. *Analytical chemistry* **2013,** *85*, 7980-7986.

33. Liu, M.; Chao, J.; Deng, S.; Wang, K.; Li, K.; Fan, C. Dark-field microscopy in imaging of plasmon resonant nanoparticles. *Colloids and Surfaces B: Biointerfaces* **2014,** *124*, 111-117.
34. Liu, X.; Wu, Z.; Zhang, Q.; Zhao, W.; Zong, C.; Gai, H. Single gold nanoparticle-based colorimetric detection of picomolar mercury ion with dark-field microscopy. *Analytical chemistry* **2016,** *88*, 2119-2124.
35. Sanchez, A.; Trappier, S. G.; Mahy, B.; Peters, C. J.; Nichol, S. T. The virion glycoproteins of Ebola viruses are encoded in two reading frames and are expressed through transcriptional editing. *Proceedings of the National Academy of Sciences* **1996,** *93*, 3602-3607.
36. Mellema, M.; Van Opheusden, J.; Van Vliet, T. Relating colloidal particle interactions to gel structure using Brownian dynamics simulations and the Fuchs stability ratio. *The Journal of chemical physics* **1999,** *111*, 6129-6135.
37. Mackay, C. E.; Johns, M.; Salatas, J. H.; Bessinger, B.; Perri, M. Stochastic probability modeling to predict the environmental stability of nanoparticles in aqueous suspension. *Integrated Environmental Assessment and Management: An International Journal* **2006,** *2*, 293-298.
38. Sandkühler, P.; Sefcik, J.; Lattuada, M.; Wu, H.; Morbidelli, M. Modeling structure effects on aggregation kinetics in colloidal dispersions. *AIChE journal* **2003,** *49*, 1542-1555.
39. Deaconu, M.; Tanré, E. Smoluchowski's coagulation equation: probabilistic interpretation of solutions for constant, additive and multiplicative kernels. *Annali della Scuola Normale Superiore di Pisa-Classe di Scienze* **2000,** *29*, 549-579.
40. Midelet, J.; El-Sagheer, A. H.; Brown, T.; Kanaras, A. G.; Werts, M. H. The sedimentation of colloidal nanoparticles in solution and its study using quantitative digital photography. *Particle & Particle Systems Characterization* **2017,** *34*, 1700095.
41. Trantidou, T.; Elani, Y.; Parsons, E.; Ces, O. Hydrophilic surface modification of PDMS for droplet microfluidics using a simple, quick, and robust method via PVA deposition. *Microsystems & nanoengineering* **2017,** *3*, 1-9.

Supplementary information for

Rapid Electronic Diagnostics of Ebola Virus with Synthetic Nanobody-Conjugated Gold Nanoparticles

Xiahui Chen[1,2,3], Shoukai Kang[4,5], Ashif Ikbal[1,2,3], Zhi Zhao[1,2,6], Jiawei Zuo[1,3], Yu Yao[1,3], Liangcai Gu[4,5], Chao Wang[1,2,3*]*

[1]*School of Electrical, Computer and Energy Engineering, Arizona State University, Tempe, AZ 85287, USA*

[2]*Center for Molecular Design and Biomimetics at the Biodesign Institute, Arizona State University, Tempe, AZ 85287, USA*

[3]*Centre for Photonic Innovation, Arizona State University, Tempe, AZ 85287, USA*

[4]*Department of Biochemistry, University of Washington, Seattle, WA 98195, USA*

[5]*Institute for Protein Design, University of Washington, Seattle, WA 98195, USA*

[6]*Current Address: College of Materials Science and Engineering, Key Laboratory of Advanced Functional Materials, Education Ministry of China, Beijing University of Technology, Beijing 100124, China*

1. Finite-difference time-domain (FDTD) simulation of AuNP extinction

We performed FDTD simulation of different numbers of AuNPs in a cluster (Figure S2). We found the resonance peaks red shift for small clusters, but the resonance becomes less evident for even larger clusters, e.g. more than 10 AuNPs. This effect is expected to be related to inter-particle coupling. It also indicates that the experimentally observed extinction is likely mainly attributed to small clusters and AuNP monomers.

2. UV-visible extinction spectra characterization of 60 nm AuNP drop cast assay in detecting sGP in 1 × PBS

Similar to the UV-visible extinction spectra characterization of 80 nm AuNP assay drop cast on glass slide as discussed in main context, Drop cast samples of 60 nm AuNP (0.086 nM) assay were also characterized by Horiba iHR 320 UV-visible spectrometer using 10 × objective lens in Olympus BX53 microscope. The measured result is shown in Figure S3.

3. Detection speed test for AuNP assay with different AuNP diameter

To investigate the detection speed for AuNP assay with different AuNP diameter, we conducted time dependent dynamic test for extinction of AuNP assay in detecting 10 nM sGP in 1×PBS. The AuNP concentrations for 40, 60, 80 and 100 nm were 0.275, 0.086, 0.036 and 0.019 nM. The measurement results are shown in Figure S4. We also note the assay time for smaller NPs (here 40 nm) tend to be less consistent compared to larger sizes. The extinction drop rate at linear region (fit in red line) for 40, 60, 80 and 100 nm AuNP is 0.049, 0.071, 0.080 and 0.091 hr^{-1}. The increasing extinction drop rate for bigger AuNP diameter is consistent with increased sedimentation velocity for larger AuNP as estimated from Mason-Waver equation [1]. This indicates that quicker precipitation can speed up the depletion of AuNP monomers resulted from unbalancing the reaction equilibrium to forward direction.

4. Characterizations of 100 nm AuNP drop cast assay in detecting sGP in 1 × PBS

100 nm AuNP assay samples were drop cast on 1mm glass slides and characterized by UV-visible spectrometer, SEM and dark field scattering imaging, as shown in Figure S5. The 100 nm AuNP concentration in assay colloid was 0.019 nM. The characterizations followed protocols described in main context method: UV-visible spectra, SEM imaging and dark field scattering imaging characterizations.

5. Drop cast samples preservation in prolonged period

We tested extinction of 80 nm AuNP assay in detecting sGP in 1×PBS (1 pM to 1 μM, in logarithmic scale) over 12 weeks (Figure S6). It can be observed that the quantitative detection results were retained over 12 weeks. The extinction especially for lower sGP concentration increased at over six weeks. This is likely due to shrinking of drop cast spot from long term dehydration as the sample exposed to dry air. The

extinction spectra were measured by 10 × objective lens in Olympus BX53 microscope coupled to Horiba iHR 320 UV-visible spectrometer.

6. Simplified modeling of AuNP assay sensing mechanism

Here we adapted the Smoluchowski's coagulation equation and modified the equation to describe our reversible AuNP aggregation process. The modified equation is:

$$\frac{dn_i}{dt} = \frac{1}{2}\sum_{j=1}^{i-1} k_{i-j,j} n_{i-j} n_j - \sum_{j=1}^{\infty} k_{i,j} n_i n_j + k_{off} n_{i+1} - k_{off} n_i \quad (1)$$

Where $n_i(t)$ is the concentration of aggregates consisting of i AuNPs, $k_{i,j}$ is the coagulation kernel for the aggregation of clusters consisting of i AuNPs and j AuNPs, k_{off} is the dissociation constant of sGP49-sGP conjugation (k_{off}=1.88×10^{-4} s^{-1}). According to Brownian diffusion theory, the coagulation kernel $k_{i,j}$ is described as [2, 3]:

$$k_{i,j} = \frac{2}{3} P \frac{k_B T}{\eta} (ij)^{\gamma} \left(m_i^{\frac{1}{d_f}} + m_j^{\frac{1}{d_f}} \right) \left(m_i^{-\frac{1}{d_f}} + m_j^{-\frac{1}{d_f}} \right) \quad (2)$$

Where P is the probability of aggregation per collision and is proportional to sGP coverage on AuNP surfaces (estimated as 0.0165 according to k_{on}=4.07×10^4 M^{-1}s^{-1}), k_B is Boltzmann constant, T is temperature, η is dynamic viscosity of colloid buffer (~1.7×10^{-3} N·s/m^2 for 20% glycerol in water), i and j are numbers of AuNP in each cluster, m_i and m_j are mass of each clusters, d_f is the fractal dimension (~2.1 for a typical densely aggregated cluster). In equation 1, The first two terms in the right side directly come from Smoluchowski's equation that describe the AuNP aggregation process. The rest two terms on the right side are added terms to describe the reversible dissociation of AuNP aggregates. For simplification, we only considered the dissociation of cluster with N number AuNPs to cluster of N-1 and a monomer released back to colloid (N → N-1,1). Although the breakdown of clusters to clusters with other arbitrary numbers of AuNPs is possible (N → N-i, i), such breakdown requires multivalent sGP-sGP49 dissociation, hence the effective dissociation rate is likely to be k_{off}^i, which is significantly smaller than k_{off}. Moreover, a further simplification of the model by only considering the low-order oligomers and monomers interactions is justified by the fact that concentration of n_i with higher i numbers (higher order) is small due to precipitation. Therefore, we could calculate the AuNP monomer concentration based on the simplified equation set and thus estimate the extinction signals by considering only the low-order oligomer-monomer interactions. This assumption is especially valid at the beginning when assay is mixed with sGP protein, where concentration of higher order oligomers and large clusters is near 0. Figure 5a shows the schematic of low-order oligomer-monomer interaction and the evolution of large clusters formation. Our simplified model follows such evolution and the equation sets are shown below:

$$\frac{dn_1}{dt} = -2k_{11}{n_1}^2 - \sum_{i=2}^{\infty} k_{1i}n_i n_1 + 2k_{off}n_2 + \sum_{i=3}^{\infty} k_{off}n_i \quad (3)$$

$$\frac{dn_2}{dt} = 2k_{11}{n_1}^2 - k_{12}n_1 n_2 + k_{off}n_3 - 2k_{off}n_2 \quad (4)$$

$$\frac{dn_3}{dt} = k_{12}n_1 n_2 - k_{13}n_1 n_3 + k_{off}n_4 - k_{off}n_3 \quad (5)$$

…

$$\frac{dn_i}{dt} = k_{1i-1}n_1 n_{i-1} - k_{1i}n_1 n_i + k_{off}n_{i+1} - k_{off}n_i \quad (6)$$

By solving the equations above, we achieved the monomer concentration versus time for 0.036 nM AuNP colloid in detecting 10 nM sGP case and converted the concentration to extinction, as shown in Figure 5b black curve. Intuitively, the solver of this equation set showed that the monomer concentration versus time is quasi-exponential based on our simplified model. The aggregation time constant τ_{agg}, defined as time required for concentration of AuNP monomer to drop to $c_{equillibrium} + \frac{1}{e}(c_0 - c_{equillibrium})$, is 0.87 hour.

Further, we calculated the monomer concentration versus time for 1.8 nM 80 nm AuNP assay in detecting 10 nM sGP. The extinction versus time is shown in Figure 5b red curve. τ_{agg} for this case is 0.024 hour, which decreases by 36.25 times compared to that of 0.036 nM AuNP assay.

(a)

Round	Input phage (Units)	Output phage (Units)
1	1.0×10^{14}	4.8×10^{6}
2	1.0×10^{12}	1.0×10^{6}
3	6.1×10^{13}	1.0×10^{8}

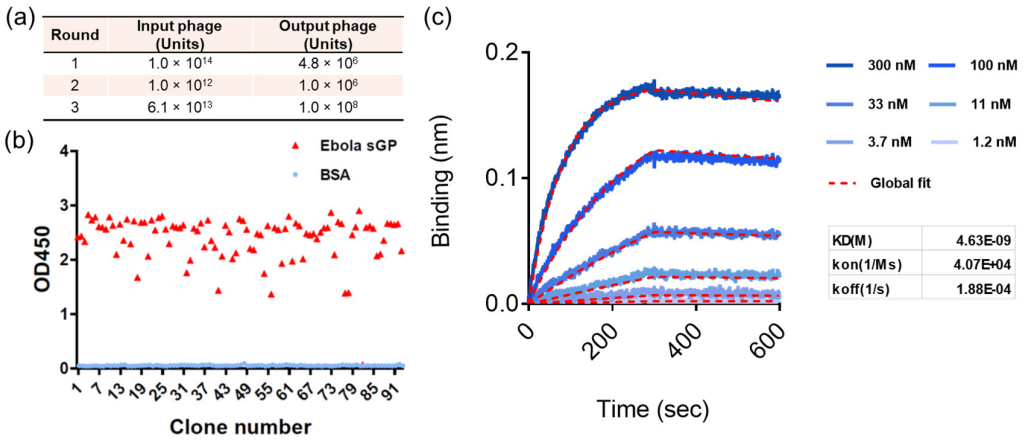

Figure S1 Nanobody selection. (a) Enrichment of phage titers following each round of biopanning. (b) ELISA results of 96 randomly picked clones after 3 rounds of selection. (c) Bio-layer interferometry analysis of sGP 49 binding kinetics.

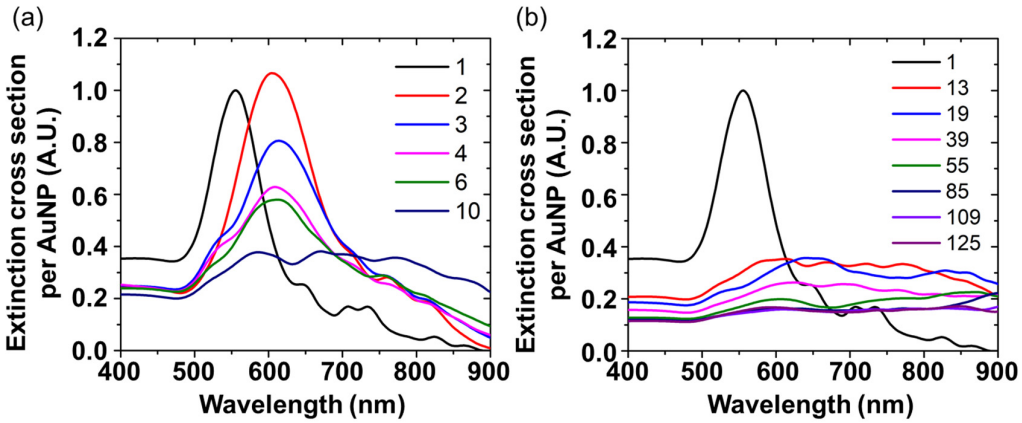

Figure S2. FDTD simulated extinction of AuNP clusters. (a) Extinction cross section of 80 nm AuNP monomer (n=1), dimer (n=2), trimer (n=3) and AuNP clusters with higher order in water. (b) Extinction cross sections for each object is normalized to AuNP monomer for comparison.

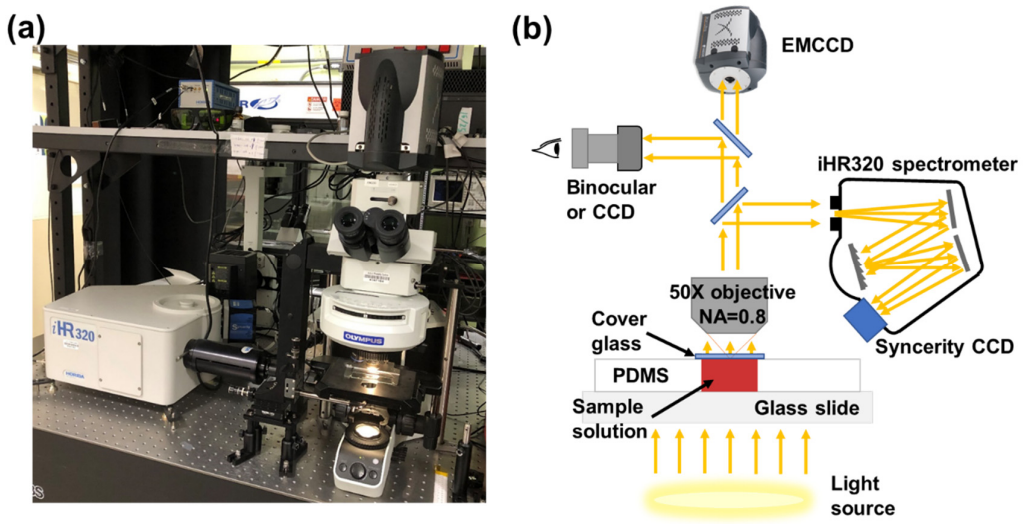

Figure S3 Experiment setup for spectrometer measurement. (a) Visual image of our lab-based UV-visible spectrometer system consisting of Horiba iHR320 spectrometer and Olympus BX53 microscope. (b) Schematic of the characterization setup for AuNP colloid-based assay using PDMS well plate as sample cuvette.

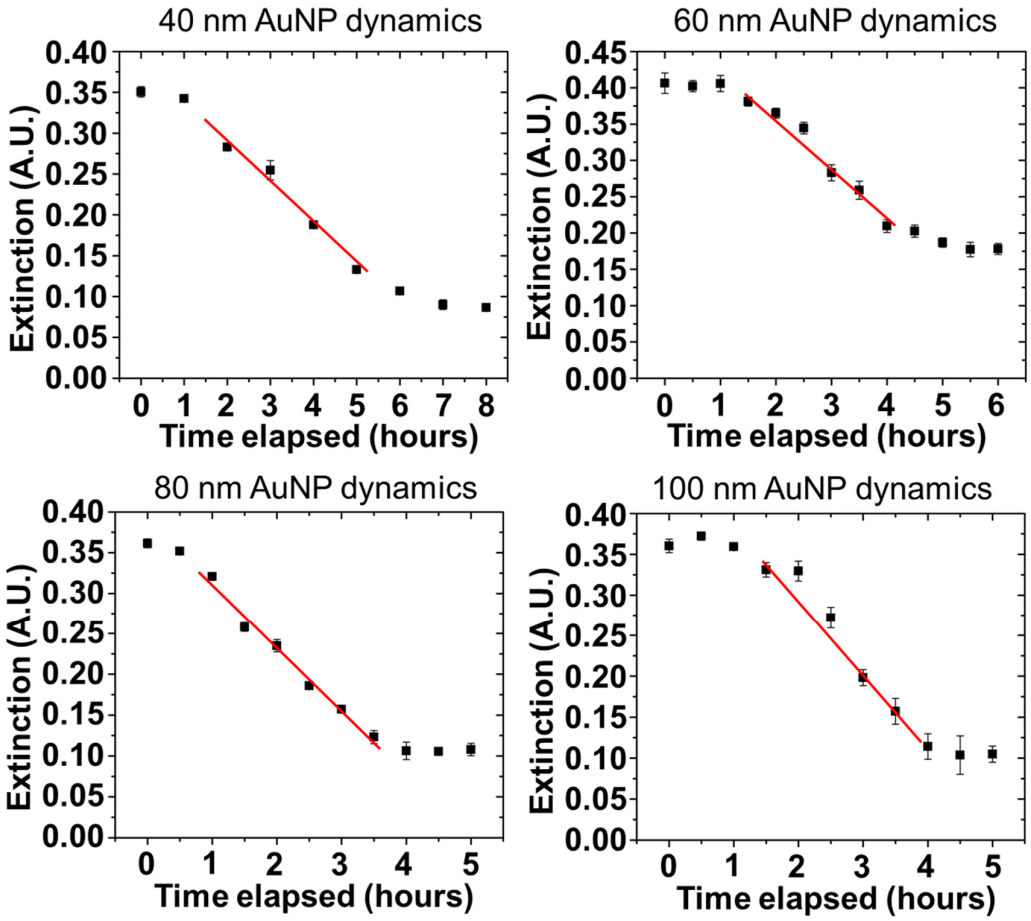

Figure S4 Time-dependent dynamic test for extinction maximum at resonance wavelength of 40, 60, 80 and 100 nm assay in detecting 10 nM sGP in 1×PBS.

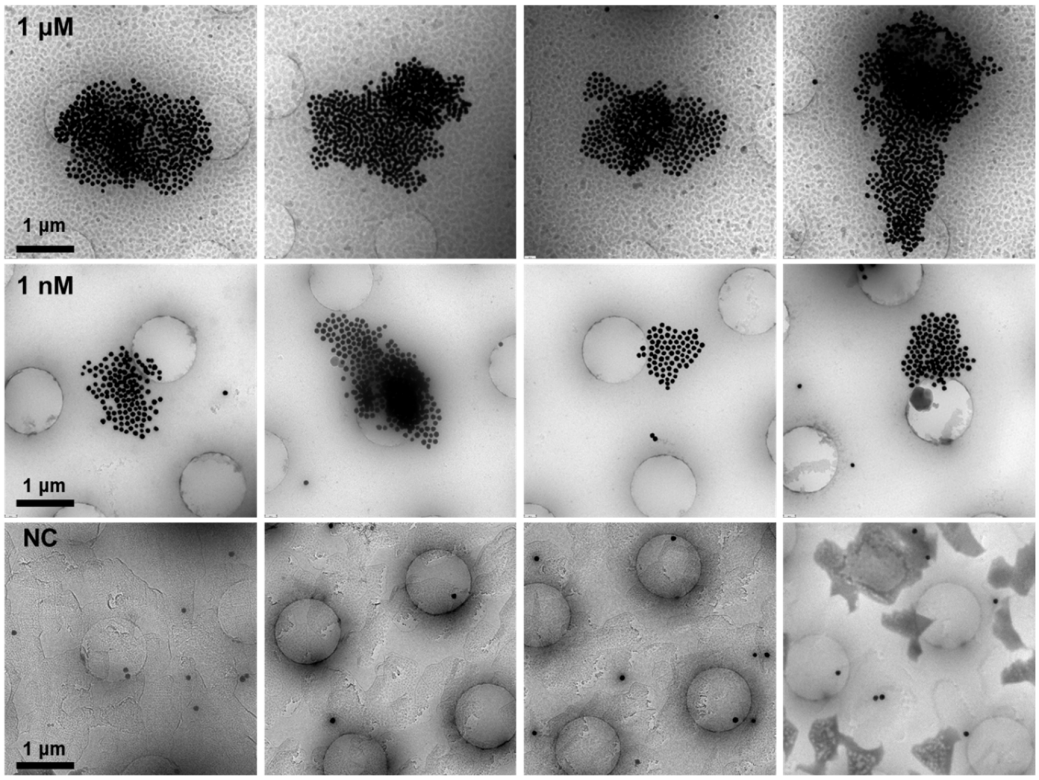

Figure S5 Representative cryoTEM images of 80 nm AuNP assay in detecting 1 nM, 1 μM sGP and NC sample.

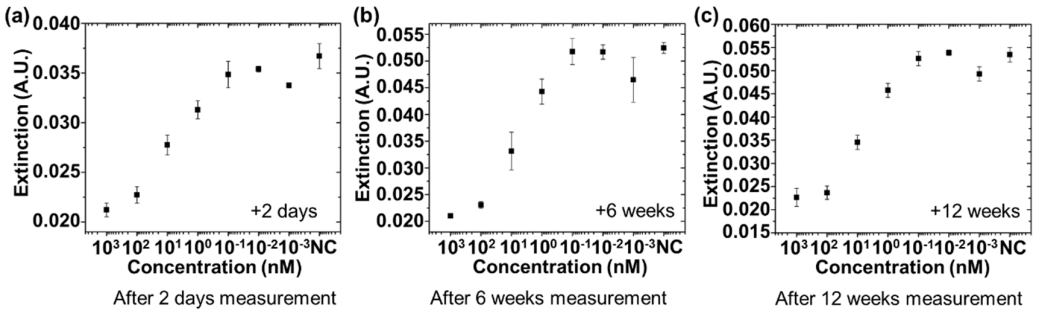

Figure S6 Extinction measurement for drop cast 80 nm AuNP assay in detecting sGP in 1×PBS (1 pM to 1 μM) on glass slide after certain period. (a) 2 days. (b) 6 weeks. (c) 12 weeks.

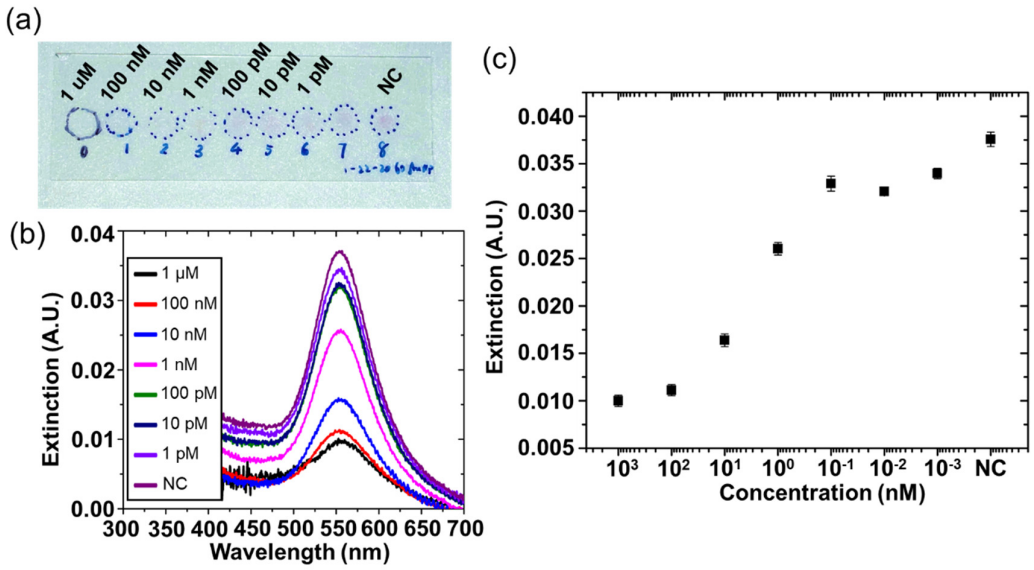

Figure S7 UV-visible spectrometer characterization of 60 nm AuNP drop cast assay. (a) Visible image of drop cast samples on 1 mm thick glass slide. (b) Extinction spectra measured for samples shown in (a). (c) Extinction maximum at AuNP resonance wavelength, extracted from extinction spectra shown in (b).

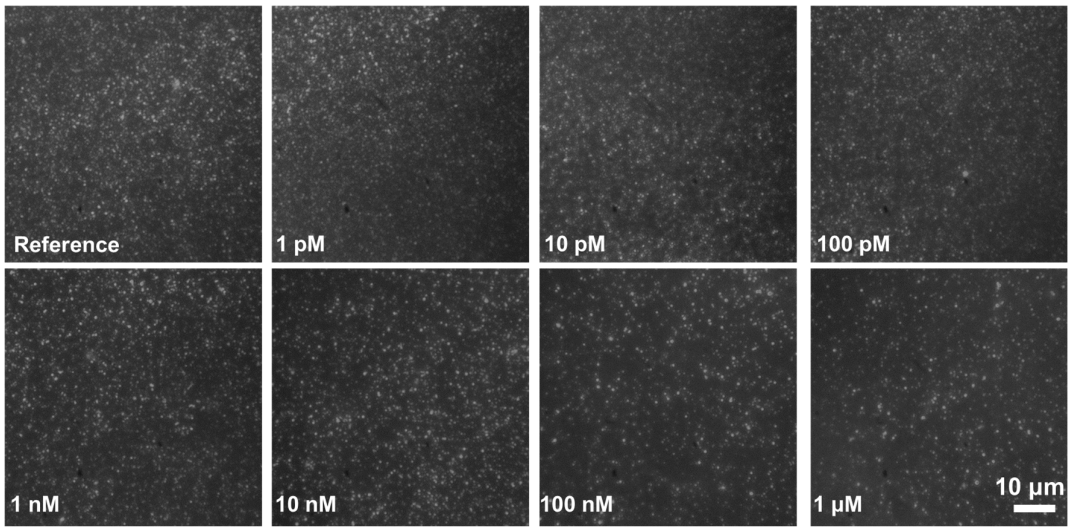

Figure S8 Dark field scattering image of 80 nm AuNP assay samples drop cast on Au surface.

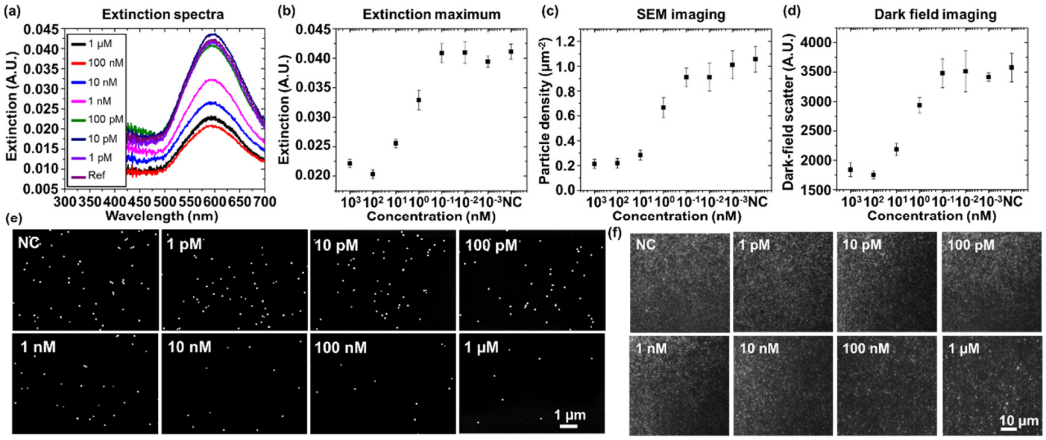

Figure S9 Characterizations of drop-casted 100 nm AuNPs. (a) Extinction spectra measured for 100 nm AuNP drop cast samples. (b) Extinction maximum at AuNP resonance wavelength, extracted from extinction spectra shown in (a). (c) Particle density averagely calculated for ten SEM images taken for 100 nm AuNP drop cast samples. (d) Scattered particle counts statistically derived for ten dark field scattering images taken for 100 nm AuNP drop cast samples. (e) SEM image of 100 nm AuNP assay samples drop cast on Au surface. (f) Dark field imaging.

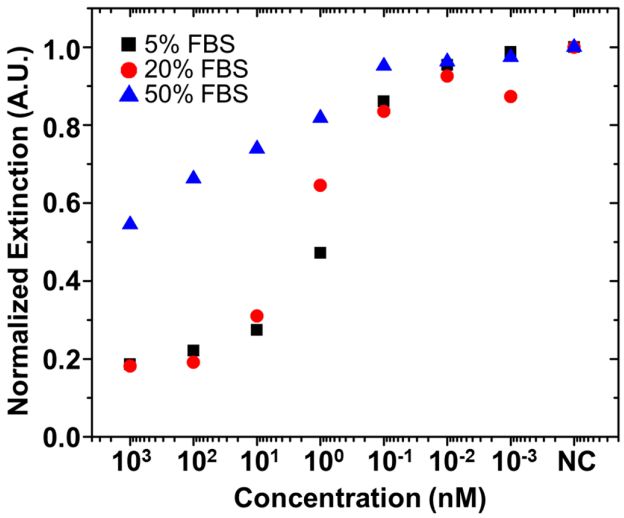

Figure S10 Normalized extinction for drop cast 80 nm AuNP assay in detecting sGP in 5, 20 and 50% fetal bovine serum. sGP concentrations were spiked from 1 pM to 1 μM.

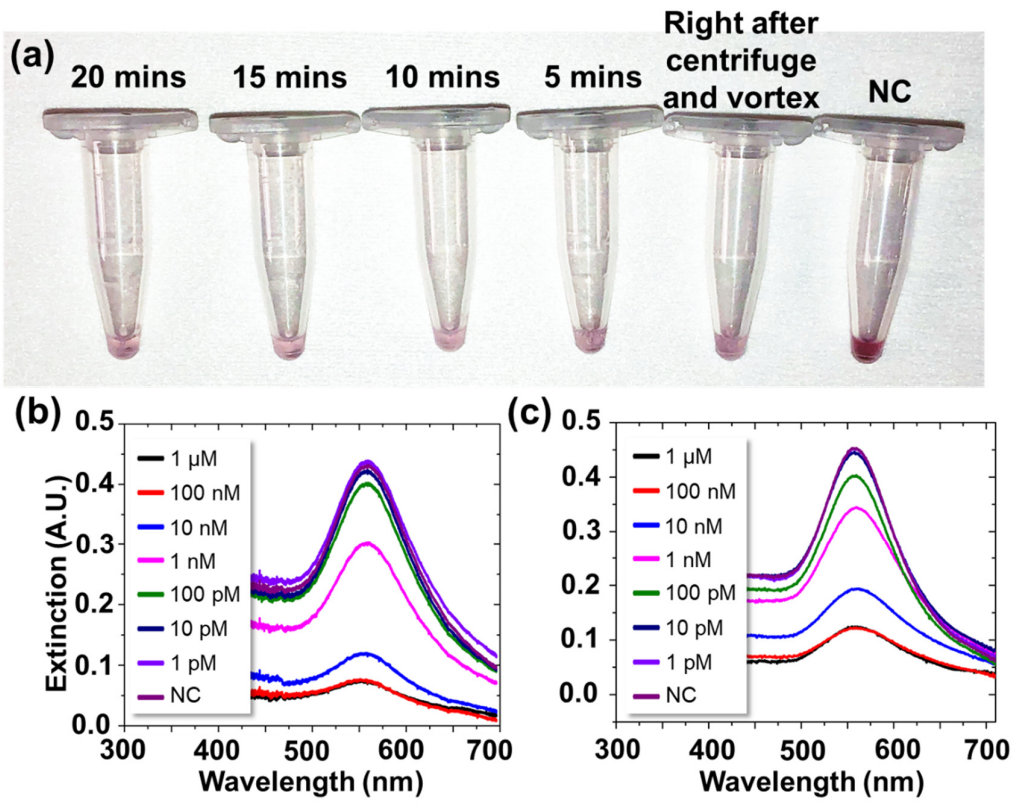

Figure S11 (a) Visual images for centrifuge enhanced 80 nm AuNP assay detecting 10 nM sGP in 1×PBS with different incubation time. (b) Extinction spectra of 80 nm AuNP assay in detecting sGP in 1×PBS with centrifugation and 20 minutes incubation time. (c) Extinction spectra of 80 nm AuNP assay in detecting sGP in 1×PBS without centrifugation and with 3 hours incubation time.

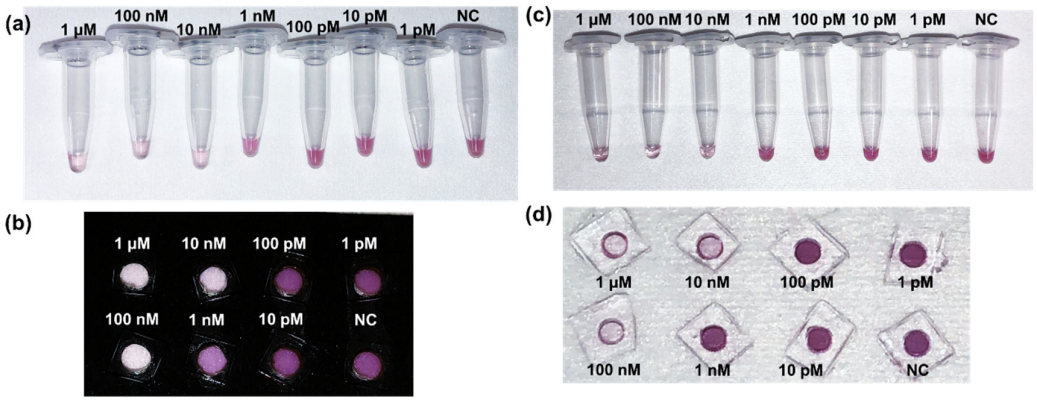

Figure S12 Visual images for 80 nm AuNP assay detecting 1 pM to 1 μM sGP in 5% FBS (a) and 1×PBS (c), with 1 min centrifugation and 15 seconds vortex. Assay supernatants in (a) were loaded in 4 mm wells on a 3mm thick PDMS well plate, as shown in (b). The region in absence of assay was covered by black flocked paper (Thorlabs, BFP1) that absorb 99% light from 420 nm to 650 nm. Assay supernatants in (c) were loaded in 2 mm holes on a 3 mm thick PDMS well plate, shown in (d).

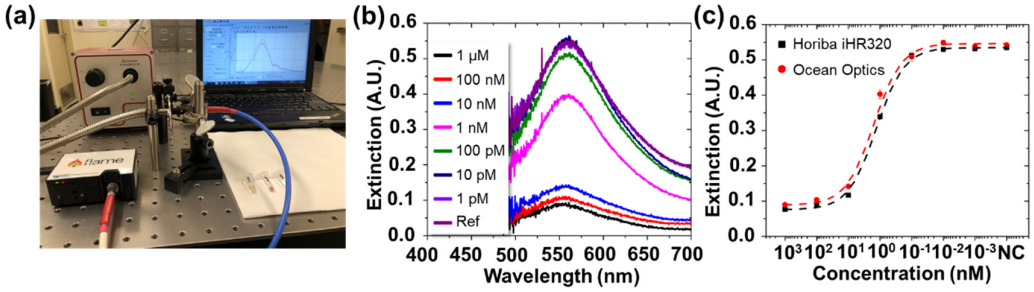

Figure S13 Demonstration of detecting sGP in fetal bovine serum using miniaturized UV-visible spectrometer system. (a) Visual image of the measurement system consisting of a laptop (right side of image), lamp source module (left side of image), Ocean Optics Flame spectrometer (right front) and alignment clamps (middle of image). The sample loaded PDMS well plate (visual images shown in Figure S12b) is placed in the gap between Ocean Optics spectrometer signal reading waveguide (right) and light source end (left). (b) Extinction spectra of assay samples in detecting sGP in 5% FBS, measured by Ocean Optics spectrometer. (c) Extinction maximum at 80 nm AuNP resonance wavelength $\lambda_p = 559$ nm, derived from spectra in (b), shown in red datapoints. Extinction maxima derived from lab-based spectrometer measured spectra (Figure S3, used 10× objective to collect transmitted light) are shown in black datapoints for comparison.

References:

1. Midelet, J.; El-Sagheer, A. H.; Brown, T.; Kanaras, A. G.; Werts, M. H., The sedimentation of colloidal nanoparticles in solution and its study using quantitative digital photography. *Particle & Particle Systems Characterization* 2017, 34, 1700095.
2. Zidar, M.; Kuzman, D.; Ravnik, M., Characterisation of protein aggregation with the Smoluchowski coagulation approach for use in biopharmaceuticals. *Soft matter* 2018, 14, 6001-6012.
3. Kim, T.; Lee, C.-H.; Joo, S.-W.; Lee, K., Kinetics of gold nanoparticle aggregation: experiments and modeling. *Journal of colloid and interface science* 2008, 318, 238-243.